Contemporary Physics

The trapped-ion qubit tool box

Roee Ozeri [a]

[a] Department of Physics of Complex Systems, The Weizmann Institute of Science, Rehovot,
76100, Israel

Available online: 27 Oct 2011

PLEASE SCROLL DOWN FOR ARTICLE

Taylor & Francis
Taylor & Francis Group

The trapped-ion qubit tool box

Roee Ozeri*

Department of Physics of Complex Systems, The Weizmann Institute of Science, Rehovot 76100, Israel

In this tutorial we review the basic building blocks of Quantum Information Processing with cold trapped atomic ions. We mainly focus on methods to implement single-qubit rotations and two-qubit entangling gates, which form a universal set of quantum gates. Different ion qubit choices and their respective gate implementations are described.

Keywords: trapped-ions; quantum computing

1. Introduction

Information is physical. Physical systems are used on a daily basis to carry out different information handling tasks. One of the most common information handling task is that of information processing, or computing.

Contemporary information processing is performed on a very large scale. We regularly consume and process enormous quantities of information. As an example, a typical 4 min long song, encoded in an mp3 format file, has a size of a few MB, which means that it needs a few tens of millions of small physical bits; systems that have two physical states that correspondingly represent the logical states 0 and 1; to be saved in memory. For music to be heard, all these bits have to be processed with many small transistors. This means that we need large arrays, of billions of physical systems which constitute all the necessary building blocks for large scale information processing. To be able to fit them all in a reasonable volume and keep power consumption on a manageable level, these physical systems have to be very small. To this end, the typical transistor size has been cut by half every two years for the past four decades. The current size of a memory cell or transistor in commercial semiconductor devices is 32 nm. We know that the physical laws that govern the behaviour of microscopic physical systems are different than those at macroscopic scales. On nanometric scales the laws of quantum mechanics often dominate.

The limitations and advantages imposed by the laws of quantum mechanics on information processing have been the focus of intensive study for the last three decades [1]. It is now widely believed that a computer,

with a performance that is completely governed by quantum mechanics, will be in principle more efficient than its classical counterpart. Its operation will certainly be very different. If a classical bit is a physical system that can be in one of two states, representing 0 or 1, a quantum bit (qubit) can be in a superposition of both. N qubits can be in a superposition of 2^N different logical states.

Quantum information processing (QIP) requires the coherent manipulation of the joint quantum state of a register of N qubits, in a 2^N dimensional Hilbert space. Some of the resulting states are highly entangled superpositions in which the superposition parts represent states that differ in many of the N qubits. For useful computations N will be mesoscopically or even macroscopically large. A superposition of two states that are macroscopically distinct was never experimentally observed and is, according to many people, even hard to envisage. The violent contrast between the superposition principle, governing the behaviour of microscopic systems, and our daily life experience at macroscopic scales was already noted in the early days of quantum mechanics [2]. The effort of realising a macroscopic quantum computer is thus also (and primarily) an effort to advance the superposition principle onto a macroscopic scale and hence it enjoys the unique position of having both practical as well as fundamental importance.

Among the many systems studied as a possible QIP platform, trapped-ions have many advantages. Atomic ions can be trapped by electric fields in ultra-high vacuum and then laser-cooled to extremely low temperatures. Figure 1 shows a linear crystal of eight,

---

*Email: ozeri@weizmann.ac.il

trapped and laser-cooled, ^{88}Sr$^+$ions. Owing to their high degree of separation from any thermal environment, quantum superpositions of trapped-ion states have relatively long coherence times. Extremely accurate control has been demonstrated over their collective internal states [3,4]. Trapped ions can be laser-cooled to the ground-state of their confining potential, thus providing excellent control of their motion as well. Qubits have been encoded into trapped-ion states [3,4]. In the last decade or so, all the basic building blocks needed for coherent control of ion qubits were developed [5]. Several quantum algorithms have been demonstrated using up to eight or so ion qubits and, from a quantum computing point of view, the challenge that experimentalists in this field are currently facing is to find ways to scale this system up to large numbers.

The challenge of experimentally realising a large-scale quantum computer is hard, and it has many different fronts. A large-scale trapping architecture has to be developed [6], tools for applying parallel quantum gates in multiple trapping regions are needed [7], and so forth. One particular challenge is to be able to drive high-fidelity coherent operations on a collective quantum state of a large number of ion qubits. Obviously, the larger the quantum register is, the larger is the space of possible quantum operations. However, the number of possible operations in a quantum code has to be finite, and in particular, independent of the number of qubits in the register. This problem is analogous to the problem of efficiently compiling a computer program into a machine code that implements physical logical operations on a logical register of bits, in a classical computer. In QIP, a finite set of unitary operations, which can be concatenated to approximate any operation on an arbitrarily large qubit register, is called a universal quantum gate set. This tutorial reviews the basic building blocks of quantum computing operations with trapped-ion qubits, with an emphasis on ways to implement a universal quantum gate set.

1.1. Universal gate set

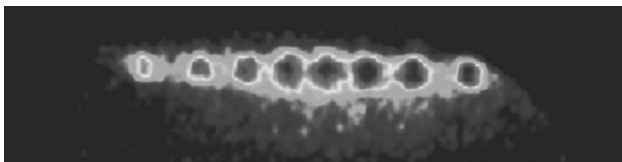The perfect coherent control of a quantum state in a 2^N dimension Hilbert space requires the ability, up to a global phase, to unitarily connect any two state vectors in this space. This seems to be a horrendous task, considering that any such unitary operator is generated by $2^{2N} - 1$ independent generators. Fortunately, it was shown that any such operation can be approximated to an arbitrary precision by concatenating a finite number of operators chosen from a small (i.e. of size which is independent of N) set [8,9]. This small and finite set of operators is called a universal set of quantum gates.

Up to a global phase, a pure quantum state of a single qubit can be visualised as a vector pointing at the surface of a sphere called the Bloch sphere, illustrated in Figure 2. Any unitary single qubit operation is therefore equivalent to a rotation $R \equiv R(\beta,\phi,\theta)$ of the Bloch vector. This rotation is specified by the three Euler angles β, ϕ, and θ. The angles $-\pi/2 < \beta < \pi/2$, and $0 < \phi < 2\pi$ determine the direction of $\boldsymbol{n} = (\cos\beta \cos\phi, \cos\beta \sin\phi, \sin\beta)$, the axis around which the Bloch vector is rotated, and θ is the rotation angle. In the Hilbert space of a single qubit, rotations are represented by *SU[2]* operators, i.e. 2×2 unitary matrices with a unity determinant. These rotations are generated by the three Pauli matrices $\hat{\sigma}_x$, $\hat{\sigma}_y$ and $\hat{\sigma}_z$. The rotation R is therefore represented by the operator,

$$\hat{R}(\beta, \phi, \theta) = \hat{R}(\boldsymbol{n}, \theta) = \exp\left(\frac{-i\hat{\sigma} \cdot \boldsymbol{n}\theta}{2}\right)$$
$$= \begin{bmatrix} \cos\frac{\theta}{2} - in_z\sin\frac{\theta}{2} & (-in_x - n_y)\sin\frac{\theta}{2} \\ (-in_x + n_y)\sin\frac{\theta}{2} & \cos\frac{\theta}{2} + in_z\sin\frac{\theta}{2} \end{bmatrix},$$

$$(1)$$

where $\hat{\sigma}$ is the Pauli operators vector.

Figure 1.   A linear crystal of eight trapped, and laser cooled ^{88}Sr$^+$ions.
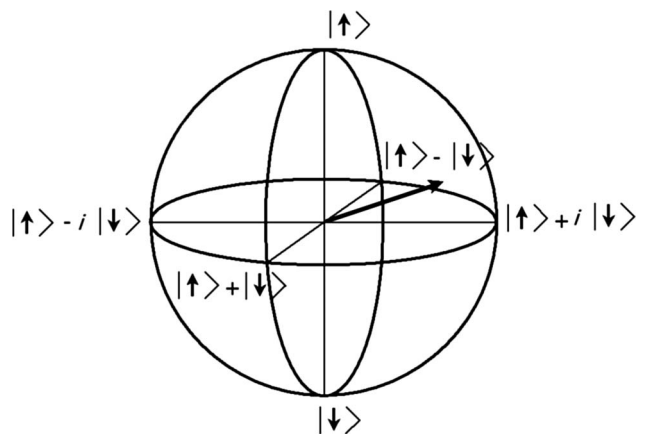

Figure 2.   All pure states of a single qubit can be geometrically described as all the points on the surface of a sphere, called the 'Bloch sphere'. All possible single-qubit operations are therefore equivalent to rotations in three dimensions.

Deutsch was the first to propose the quantum Toffoli gate [8], a rotation $\hat{R}$ of a single target qubit which is conditioned on the state of two control qubits, as a universal gate set (see Figure 3(*a*)). Here the state of the target qubit undergoes a rotation $\hat{R}$ if and only if the state of both control qubits is in the logical $|1\rangle$. Later, Barenco and co-authors proved that single qubit rotations, $\hat{R}$, together with two-qubit controlled-not (CNOT) gates, shown diagrammatically in Figure 3(*b*), are a universal quantum gate set as well [9]. A CNOT quantum gate performs a $\theta = \pi$ rotation of the target qubit around the Bloch sphere *x*-axis, i.e. $\hat{R} = \hat{\sigma}_x$, only if the control qubit is in state $|1\rangle$. Both of these gate set examples are not finite since $\hat{R}$ is defined through continuous parameters. It has been shown, however, that by restricting to a small set of rotation angles, any single qubit rotation, $\hat{R}$, can be approximated to accuracy ε by concatenating a string of length $\log^c(I/\varepsilon)$, where c is a constant, approximately equal to 2, of operators from the small set above [1,10].

1.2. QIP with trapped ions

Qubits that are encoded in the internal states of laser-cooled and trapped ions are promising candidates as a quantum computing platform [3]. Trappedions are well isolated; thus the coupling of environmental noise to their internal electronic states is weak. The long

Figure 3. Quantum circuits of universal gate sets. (*a*) The Toffoli gate is a controlled rotation. The state of a target qubit is rotated only if the state of both control qubits is in the logical $|\uparrow\rangle$. (*b*) Single-qubit rotations and controlled-not (CNOT). In a CNOT gate the state of a target qubit is rotated by 180° around the *x*-axis, if the state of the control qubit is in the logical $|\uparrow\rangle$.

coherence time attainable with atomic superpositions has been long recognised and led to the development of atomic time standards [11]. Manipulation of atomic superpositions with electro-magnetic radiation has been extensively studied [12]. Single atomic-qubit rotations were demonstrated long before the emergence of quantum information science (e.g. [13]).

In a seminal paper Cirac and Zoller proposed a method to implement a CNOT gate between ion qubits by using their long-range Coulomb interaction [14]. In the last few years, different schemes for implementing quantum gates that can serve as parts of a universal set were theoretically suggested [15–19] and experimentally demonstrated on trapped-ion systems with high fidelity [20,21].

In this tutorial we review some of the current methods for implementing a universal quantum gate set on trapped ion qubits. Here we will focus on the universal gate set suggested in [9], i.e. single qubit rotations and two-qubit CNOT gates. In Section 2 we review different ion qubit choices, in Section 3 we outline methods of implementing single qubit rotations on the various qubit choices. Finally, in Section 4 we describe a method for implementing a two-qubit entangling gate. Here we focus on a two-qubit phase gate that is based on spin-dependent light forces.

2. The ion qubit

Quantum information is encoded in the internal electronic levels of trapped ions. Ions with a single electron in the valence shell have a relatively simple level structure and are therefore well suited for this purpose. The relatively manageable electronic level structure also simplifies the laser-cooling of such 'alkali-like' ions. Once singly ionised, all the elements with stable isotopes in group A II earth alkalies, Be^+, Mg^+, Ca^+, Sr^+, and Ba^+, are good candidate ions with a single electron in the zero angular momentum orbital, S, of the *n*th electronic level. All of these ions have filled S and P orbitals at the $(n - 1)$ level and no electrons in the D orbital of the $(n - 1)$ level, if they are heavy enough to have one. All the radioactively stable, singly ionised, group B II transition metals, Zn^+, Cd^+ and Hg^+, qualify, with $(n - 1)$ filled S, P, and D orbitals and a single electron at the n S level. Finally, the only singly ionised lanthanide with a single electron in the valence shell is Yb^+, with filled $(n - 1)$ S and P and $(n - 2)$ F orbitals and a single electron at the n S level. The trapping and laser-cooling of all ions mentioned above were demonstrated [22–30].

Since it is only singly ionised 'alkali-like' ions that are currently used for QIP purposes, it is worthwhile reviewing common features in their internal level structure. Figure 4 shows a schematic diagram of the
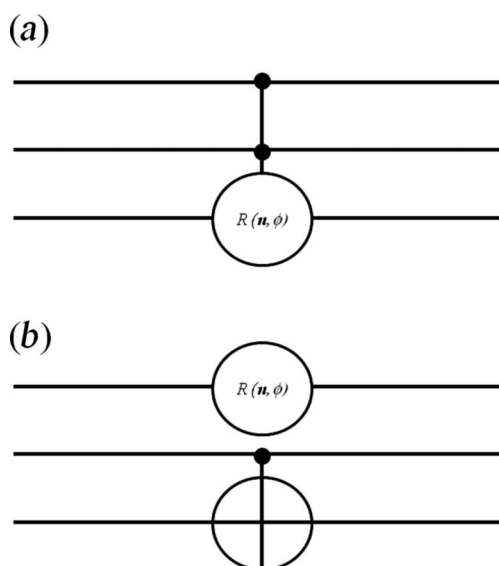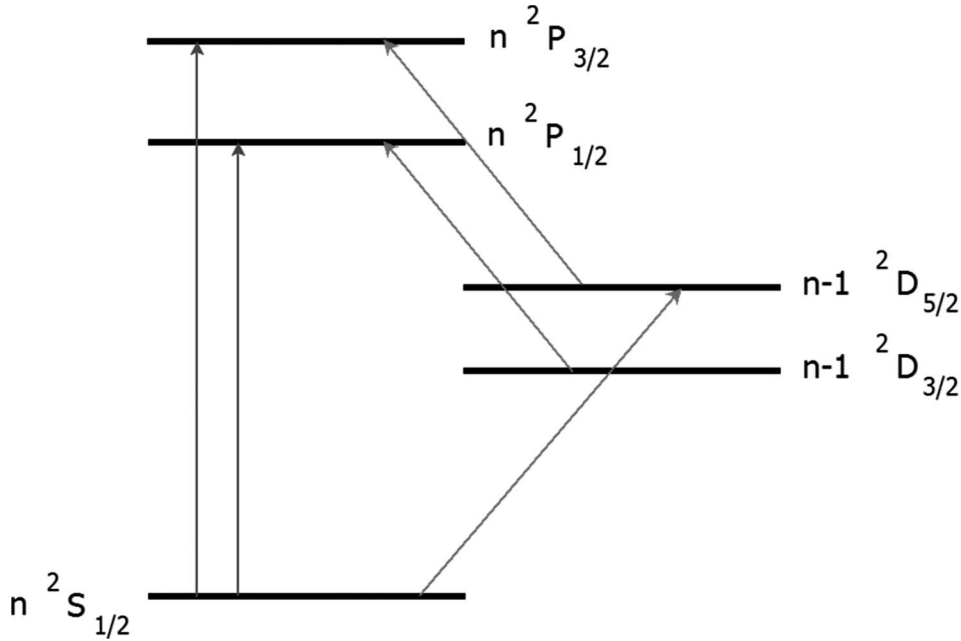
Figure 4. A diagram of the typical level structure of singly ionised 'alkali-like' ions. The ground electronic state is the zero angular momentum orbital, S, of the n th electronic level. An electric–dipole allowed transition to the P orbital (typically in the blue-ultraviolet range) allows for laser-cooling, optical pumping and state-selective fluorescence detection. In those ions that are heavy enough to have a D orbital in the $(n - 1)$ th electronic level, a narrow electric–quadrupole transition allows for the realisation of an optical qubit.

first few levels of such 'alkali-like' ions. The ground electronic state of the valence electron is $ns^2 S_{1/2}$, where n is the valence shell principal quantum number and S is the zero angular momentum orbital. The electron can be optically excited to the P orbital via an electric–dipole transition. Owing to spin–orbit coupling, the P orbital splits into two fine-structure levels: $np^2 P_{1/2}$ and $np^2 P_{3/2}$. Table 1 lists the $S_{1/2} \rightarrow P_{1/2}$ and $S_{1/2} \rightarrow P_{3/2}$ transition wavelengths and the natural spectral width of the $P_{1/2}$ levels for the various ions.

Earth alkaline ions heavy enough to have a D orbital in the $(n - 1)$ shell (Ca^+, Sr^+, and Ba^+, as well as Hg^+ and Yb^+), have the $nd^2 D_{3/2}$ and $nd^2 D_{5/2}$ fine-structure levels between the S and the P levels. Since the S and the D orbitals both have even parity, the electric–dipole transition is forbidden and the two levels are coupled only through their electric–quadrupole moment. The lifetime of the D levels (and hence the natural width of the $S \rightarrow D$ transition) is therefore long (narrow), and typically of the order of one second (one Hz). The $D \rightarrow P$ transition is an electric dipole transition and therefore, once excited to the P level, the electron can decay both to the states in the S as well as in the D levels with a fixed branching ratio, f. The $S \rightarrow P$ transition is typically used for laser-cooling and other QIP manipulations, and in those ions that have low-lying D levels, re-pumping lasers, e.g. with a wavelength that is tuned to the $D \rightarrow P$ transition, are

Table 1. A list of atomic constants of several of the hyperfine-ion qubits. Here I is the nuclear spin, γ is the natural width of the $P_{1/2}$ level, Δ_{hf} is the $S_{1/2}$ hyperfine splitting, $\lambda_{1/2}$ and $\lambda_{3/2}$ are the $S_{1/2} \rightarrow P_{1/2}$ and $S_{1/2} \rightarrow P_{3/2}$ transition wavelengths, respectively.

Ion	I	$\gamma/2\pi$ (MHz)	Δ_{hf} (GHz)	$\lambda_{1/2}$ (nm)	$\lambda_{3/2}$ (nm)
$^9Be^+$	3/2	19.6	1.25	313.1	313.0
$^{25}Mg^+$	5/2	41.3	1.79	280.3	279.6
$^{43}Ca^+$	7/2	22.5	3.23	396.8	393.4
$^{67}Zn^+$	5/2	62.2	7.2	206.2	202.5
$^{87}Sr^+$	9/2	21.5	5.00	421.6	407.8
$^{111}Cd^+$	1/2	50.5	14.53	226.5	214.4
$^{137}Ba^+$	3/2	20.1	8.04	493.4	455.4
$^{171}Yb^+$	1/2	19.7	12.64	369.4	328.9
$^{199}Hg^+$	1/2	54.7	40.51	194.2	165.0

necessary to prevent the ion from remaining in the long-lived D manifold.

In odd isotopes or even isotopes with non-zero nuclear spin, $I \neq 0$; all the above levels are split into two or more hyperfine manifolds. A small magnetic field usually splits these manifolds further into different Zeeman sub-levels.

A qubit is best encoded in a pair of levels that are as resilient as possible to decay and decoherence. Since levels in the P manifold have a very short lifetime (in the few nS range), qubit levels are typically encoded in

two $S_{1/2}$ states or a S and D superposition. Three typical choices for an ion qubit are discussed below.

2.1. Zeeman qubit

Encoding a qubit in a pair of $S_{1/2}$ levels has the advantage of a practically infinite spontaneous decay time. In ions where $I = 0$, the only states in the $S_{1/2}$ level are the two Zeeman states corresponding to the valence electron spin pointing parallel and anti-parallel to the external magnetic field direction [31]. The energy splitting between the qubit levels is $g_s \mu_B B \simeq 28$ MHz mT^{-1}. Here g_s is the bound electron g-factor, μ_B is Bohr magneton and B is the magnetic field magnitude. An advantage of choosing this qubit is that since the qubit levels are the only levels in the $S_{1/2}$ manifold, optical pumping out of the qubit manifold does not occur. One obvious drawback of the Zeeman qubit is that since the energy difference between the two qubit states depends linearly on the magnetic field, magnetic field noise will cause dephasing. Furthermore, at low magnetic fields the frequency separation between the two qubit states is smaller than the P level natural spectral width and therefore state selective fluorescence cannot be directly applied for qubit state detection.

2.2. Hyperfine qubit

In odd isotopes or even isotopes with non-zero nuclear spin, $I \neq 0$, the $S_{1/2}$ is split into $(4I + 2)$ different m_F states in two hyperfine manifolds: $F = I \pm 1/2$. A qubit can be encoded in any pair of hyperfine states [32–36]. The manifolds are split at a low magnetic field by $\Delta_{hf} = (I + 1/2)A_{hf}$, where A_{hf} is the ground-state hyperfine constant, which for all the ions discussed here is in the few GHz range. Table 1 lists Δ_{hf} values for various hyperfine ion qubits. A small magnetic field removes the degeneracy between different Zeeman states in each of the two manifolds. The Zeeman shift at a low magnetic field is given by $g_F \mu_B B m_F$, and at all magnetic field levels it can be analytically calculated from the Breit–Rabi formula [37]. A clear advantage of the hyperfine qubit choice is that pairs of levels can be found such that their energy separation does not depend, to first order, on the magnetic field. The most commonly used example is the $|F = I + 1/2, m_f = 0\rangle$ and $|F = I - 1/2, m_f = 0\rangle$ states at zero magnetic field, often referred to as the 'clock transition' states. Working exactly at zero magnetic field is not feasible since the degeneracy between different Zeeman states has to be removed to enable spectroscopic addressing of various transitions. Consequently, at a low non-zero field, B_0, the magnetic field dependence of the clock transition is first order but small. At certain magnetic fields, large enough such that the magnetic dipole

energy is comparable with $\hbar A_{hf}$, other transitions can be found that are first order insensitive to magnetic field variations [38].

2.3. Optical qubit

Ions that have a low-lying D level have the possibility of encoding a qubit into levels connected by the $S \rightarrow D$ optical transition. Since the lifetime of the D level is typically of the order of a second, the fundamental limit to the optical qubit coherence time is long relative to a typical operation time. However, in contrast with the two previously discussed qubit choices where the local oscillator is in the radio frequency (RF) or microwave range, here the local oscillator is a laser. The coherence time of the qubit is therefore also limited by a finite laser linewidth. A laser linewidth comparable to the D level natural spectral width ($\simeq 1$ Hz) requires laser fractional frequency stability of the order of 10^{-14}, a non-trivial task. This difficulty renders the optical ion qubit choice less common. In ions with $I \neq 0$ both the S and the D levels are hyperfine split. Since the $P_{1/2}$ level of ions cannot decay to the $D_{5/2}$, an optical qubit that is encoded on the $S_{1/2} \rightarrow D_{5/2}$ transition enables state-selective fluorescence on the $S_{1/2} \rightarrow P_{1/2}$ transition (see Section 2.4). Table 2 lists the $S_{1/2} \rightarrow D_{5/2}$ transition wavelengths, the $D_{5/2}$ level lifetime, and f, the branching ratio of $P \rightarrow S/P \rightarrow D$ spontaneous decay for the various ions.

2.4. Initialisation and detection

All the ion qubit choices mentioned above are initialised to a fiducial state using optical pumping techniques [3]. Qubit state detection is typically performed using state-selective fluorescence [3,39,40]. Photons are scattered from a laser beam resonant with a transition connecting one of the qubit states to a short-lived state. The scattered light is collected on a photo-detector. Whether or not the photo-detector measures light indicates the state onto which the ion qubit superposition collapses. For optical ion qubits,

Table 2. The table lists the $S_{1/2} \rightarrow D_{5/2}$ transition wavelengths, the $D_{5/2}$ level lifetime and, f, the branching ratio of $P \rightarrow S/P \rightarrow D$ spontaneous decay in various optical ion qubits.

Ion	$\lambda_{D5/2}$ (nm)	$D_{5/2}$ lifetime (s)	f
Ca$^+$	729.1	1.17	1/17
Sr$^+$	674.0	0.36	1/14
Ba$^+$	1761.7	30	1/3
Yb$^+$	411.0	0.007	1/290
Hg$^+$	281.6	0.1	1/700

state-selective fluorescence is straightforward since the two qubit levels are optically separated. For example, the ion scatters photons from a laser beam that is resonant with the $S_{1/2} - P_{1/2}$ transition [41–43]. The ion cannot decay from the $P_{1/2}$ to the $D_{5/2}$ level and therefore if the qubit superposition collapses on the $D_{5/2}$ state, then no photons are detected during the detection period. Errors in detection here will be due to background photon counts and the finite spontaneous decay probability of the $D_{5/2}$ state during the detection period. Hyperfine qubit levels are typically separated by much more than the P level's natural width (typically a few GHz as compared with a few tens of MHz; see Table 1). State-selective fluorescence is therefore possible on a cycling transition, i.e. a transition in which, due to selection rules, the P level decays only to a single S state [40,44]. Errors in this case will be mostly due to off-resonance coupling of the detection laser to unwanted states [38]. A fairly large magnetic field is needed in order to separate the two states of a Zeeman qubit by much more than the P level natural width. Hence, state-selective fluorescence cannot be used directly. Detection is typically performed in Zeeman qubits by shelving one of the qubit states on a spectrally distant meta-stable state, e.g. one of the $D_{5/2}$ states [45–47]. Other detection schemes that use quantum logic protocols to enhance detection efficiency have been demonstrated as well [48,49].

3. Single qubit gates

Single-ion qubit gates have been extensively reviewed (e.g. [3,4,50]). Here we initially provide a general description of single-ion qubit gates followed by a discussion of specific implementations for the various qubit choices.

The qubit levels are coupled by electro-magnetic (e.m.) travelling plane waves, i.e. we assume that the ion is placed in the far-field of the e.m. radiation. This assumption does not always hold, however, and there have been several proposals to implement ion qubit gates using near-field e.m. fields [3,51–55]. The qubit evolution is determined by the time-dependent Hamiltonian,

$$\hat{H}(t) = \hat{H}_0 + \hat{V}(t). \qquad (2)$$

Here $\hat{H}_0$ is the free Hamiltonian of a spin connected to a 1D harmonic oscillator (h.o.),

$$\hat{H}_0 = \frac{1}{2}\hbar\omega_0\hat{\sigma}_z + \hbar\omega_m(\hat{a}^\dagger\hat{a} + \tfrac{1}{2}), \qquad (3)$$

where ω_0 is the qubit levels frequency separation and ω_m is the h.o. frequency. The time-dependent

periodic potential $\hat{V}(t)$ is induced by coupling to the e.m. wave,

$$\hat{V}(t) = \hbar\Omega_0(\hat{\sigma}^+ + \hat{\sigma}^-)\cos(k\hat{x} - \omega t + \phi). \qquad (4)$$

The coupling constant Ω_0 is also known as the Rabi frequency and $\hat{\sigma}^{+/-}$ are the spin raising/lowering operators,

$$\hat{\sigma}_- = \hat{\sigma}_x + i\hat{\sigma}_y = |\downarrow\rangle\langle\uparrow|,$$
$$\hat{\sigma}_+ = \hat{\sigma}_x - i\hat{\sigma}_y = |\uparrow\rangle\langle\downarrow|. \qquad (5)$$

The wave-vector, frequency, and phase of the e.m. plane wave are $\boldsymbol{k}$, ω, and ϕ, respectively. The position operator can be written in terms of the h.o. creation and annihilation operators, $\hat{a}$ and $\hat{a}^\dagger$,

$$\boldsymbol{k}\hat{x} = kx_{eq} + kx_0(\hat{a}^\dagger + \hat{a}) \equiv kx_{eq} + \eta(\hat{a}^\dagger + \hat{a}). \qquad (6)$$

The phase owing to the equilibrium position of the ion, kx_{eq}, can be absorbed in ϕ. Here k is the projection of $\boldsymbol{k}$ along the trap direction, $x_0 = (\hbar/2m\omega_m)^{1/2}$ is the h.o. ground-state width and $\eta = kx_0$ is the Lamb–Dicke parameter. Moving to the interaction representation and using the rotating-wave approximation (RWA), the interaction Hamiltonian is

$$H_{int}(t) = \hbar\Omega_0/2\hat{\sigma}_+\exp$$
$$[i\eta(\hat{a}\exp(-i\omega_m t) + \hat{a}^\dagger\exp(i\omega_m t))]$$
$$\exp[i(\phi - \delta t)] + H.C. \qquad (7)$$

The RWA keeps only terms that vary slowly in time and contribute the most to time evolution under $\hat{H}_{int}$. Expanding the exponent in Equation (7) we obtain terms oscillating at multiples of ω_m. When $\delta = s\omega_m$, with integer s, only one of these terms is in resonance and dominantly contributes to the ion qubit time evolution. Here the Rabi frequency is modified to

$$\Omega_{n,n+s} = \Omega_{n+s,n} = \Omega_0\langle n+s|\exp[i\eta(\hat{a} + \hat{a}^\dagger)]|n\rangle$$
$$\equiv \Omega_0 D_{n+s,n}, \qquad (8)$$

indicating the coupling of the two qubit levels and the n and $n + s$ h.o. levels. The coupling is modified by $D_{n+s,n}$, the Debye–Waller factor. For the 1D harmonic oscillator the Debye–Waller factor is analytically calculated to be

$$D_{n+s,n} = \exp(-\eta^2/2)\eta^{|s|}\left(\frac{n_<!}{n_>!}\right)^{1/2}L_{n_<}^{|s|}(\eta^2). \qquad (9)$$

Three different cases are commonly used. The carrier transition occurs when $s = 0$ and the two qubit levels are coupled without changing the h.o. motional state.

The Hamiltonian in the interaction representation is given by

$$\hat{H}_{\text{carrier}} = \frac{\hbar\Omega_{n,n}}{2}\left(\hat{\sigma}_+\exp\left(i\phi\right) + \hat{\sigma}_-\exp\left(-i\phi\right)\right). \quad (10)$$

The red sideband (RSB) transition is the transition for which $\delta = -\omega_{\text{m}}$ ($s = -1$). Here, when the ion qubit spin state is raised, a single h.o. quantum of motion is annihilated. The interaction Hamiltonian for the RSB is

$$\hat{H}_{\text{RSB}} = \frac{\hbar\Omega_{n-1,n}}{2}\left(\hat{a}\hat{\sigma}_+\exp\left(i\phi\right) + \hat{a}^\dagger\hat{\sigma}_-\exp\left(-i\phi\right)\right). \quad (11)$$

This Hamiltonian is identical to the well-known Jaynes–Cummings Hamiltonian in quantum-optics. The third case is that of the blue-sideband (BSB) transition, where $\delta = +\omega_{\text{m}}$ ($s = +1$) and the raising of the qubit spin is accompanied by creating a single h.o. quantum,

$$\hat{H}_{\text{BSB}} = \hat{H}_{\text{int}} = \frac{\hbar\Omega_{n+1,n}}{2}\left(\hat{a}^\dagger\hat{\sigma}_+\exp\left(i\phi\right) + \hat{a}\hat{\sigma}_-\exp\left(-i\phi\right)\right). \quad (12)$$

Note that both the BSB and the RSB transitions entangle the qubit spin with its motional state.

When the deviation of the ion from its average position is much smaller than the radiation wavelength, $\eta(\langle(\hat{a}^\dagger + \hat{a})^2\rangle)^{1/2} \ll 1$, the Debye–Waller factor (9) can be expanded using η as a small parameter. In this regime, known as the Lamb–Dicke regime, the Rabi frequencies of the three cases discussed above can be approximated by

$$\Omega_{n,n} \simeq \Omega_0\left[1 - (n + 1/2)\eta^2\right], \quad (13)$$

$$\Omega_{n-1,n} \simeq \Omega_0 n^{1/2}\eta, \quad (14)$$

$$\Omega_{n+1,n} \simeq \Omega_0(n + 1)^{1/2}\eta. \quad (15)$$

The carrier Rabi frequency $\Omega_{n,n}$ is corrected by $(n + 1/2)\eta^2$, a correction that is small in the Lamb–Dicke regime. The RSB and BSB Rabi frequencies depend on the ion motion to a greater extent and are proportional to $\eta n^{1/2}$ and $\eta(n + 1)^{1/2}$, respectively. Note that the RSB Rabi frequency vanishes for $n = 0$ since no h.o. quanta can be further extracted.

The dependence of the Rabi frequencies on η and n can be understood by considering the effect of photon recoil on the overlap between different h.o. wavefunctions. Look at the overlap between a momentum-displaced h.o. ground-state, a Gaussian, and either a ground-state (carrier transition) or the

first h.o. excited state (BSB transition), shown in Figure 5. Here the wavefunction is plotted versus momentum in units of $2\pi\hbar/x_0$. In these units the h.o. ground-state width is unity whereas the momentum displacement is $\eta \ll 1$. The overlap between the ground-state and the displaced ground-state is $1 - \eta^2/2$ since the Gaussians are displaced by η around their maximal overlap point. The overlap between the displaced Gaussian and the first excited state increases linearly with η since the Gaussian peak is displaced along the excited state's linear slope. The dependence on n results from the fact that the distance between nodes in the h.o. wavefunction, and therefore also the width of each node is roughly $\hbar n^{1/2}/x_0$. The overlap between n and the displaced $n + 1$ wavefunctions would therefore also be proportional to $n^{1/2}$. The $n^{1/2}$ dependence can also be thought of as resulting from bosonic amplification.

To avoid entanglement of the ion qubit spin with its motion, on-resonance carrier transitions are used to drive single qubit gates. Here the interaction Hamiltonian, Equation (10), is time independent and the qubit

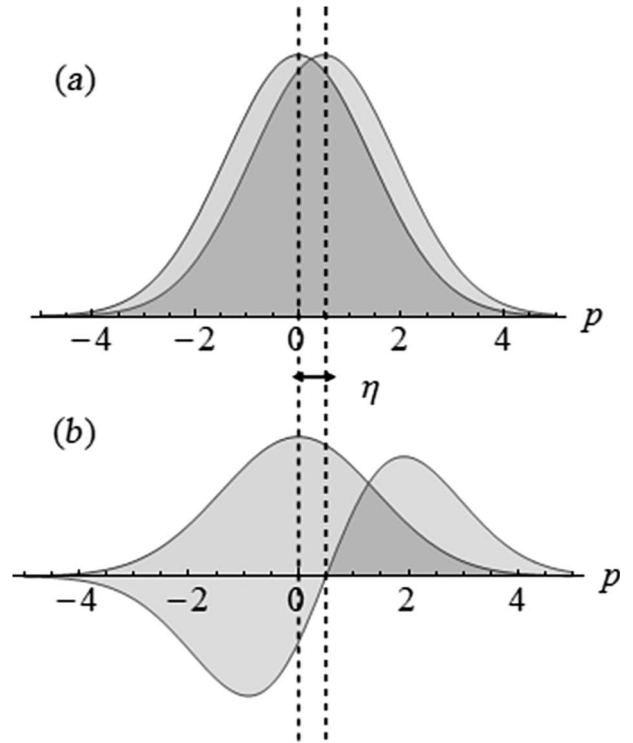Figure 5. Momentum transfer in the Lamb–Dicke regime. (a) The overlap between a harmonic-oscillator (h.o.) ground-state and the same ground-state displaced by η, owing to photon recoil, decreases by $\eta^2/2$. Here, we use the units where x_0, the ground-state width equals unity. (b) The overlap between the h.o. first excited state and the recoil displaced ground-state increases linearly with η.

time evolution in the interaction representation is given by

$$|\Psi(t)\rangle_{\text{int}} = \exp\left(-i\hat{H}_{\text{int}}t/\hbar\right)|\Psi(0)\rangle_{\text{int}}$$
$$= \exp\left(-i\theta\sigma \cdot \boldsymbol{n}\right)|\Psi(0)\rangle_{\text{int}} \equiv \hat{R}(\theta,\phi,0)|\Psi(0)\rangle_{\text{int}}. \quad (16)$$

Here $\theta = \Omega_{n,n}\, t$ and the Rabi vector direction are given by the unit vector $\boldsymbol{n} = (\cos\phi, \sin\phi, 0)$ pointing in the Bloch sphere equatorial plane. The rotation matrix $\hat{R}(0,\phi,\theta)$ represents the spinor rotation operator,

$$\hat{R}(0,\phi,\theta) = \begin{bmatrix} \cos(\theta/2) & -ie^{i\phi}\sin(\theta/2) \\ -ie^{-i\phi}\sin(\theta/2) & \cos(\theta/2) \end{bmatrix}. \quad (17)$$

The origin of the coupling, represented by Ω_0, can vary and depends on the ion qubit choice. Next, we describe three different single-qubit gate coupling implementations for the different ion qubit types.

3.1. Magnetic dipole coupling

Zeeman or hyperfine qubits have a separation between their levels that is in the RF or microwave range. The two qubit states represent different directions or magnitudes of a magnetic dipole and can therefore be coupled by inducing magnetic dipole transitions. The time-varying potential in the presence of an oscillating magnetic field is

$$V(t) = -\hat{\mu} \cdot B_0 \cos\left(k\hat{x} - \omega t + \phi\right). \quad (18)$$

The magnetic moment of the electron is $\hat{\mu} = \mu_B(g_S\hat{\boldsymbol{S}} + g_L\hat{\boldsymbol{L}} + g_I\hat{\boldsymbol{I}})$, where $\hat{S}$, $\hat{L}$, and $\hat{I}$ are the electronic spin, the electronic orbital angular momentum, and nuclear spin operators, respectively, and g_S, g_L and g_I are the corresponding g-factors. The Rabi frequency here is given by $\Omega_0 = \langle\downarrow|\hat{\mu}\cdot\boldsymbol{B}_0|\downarrow\rangle$. For a Zeeman qubit $\hat{\mu} = g_S\mu_B\hat{\sigma}$. The Rabi frequency will maximise to $\Omega_0 = 2\pi \times 28B_0$ MHz when $\boldsymbol{B}_0$ (in mT) is perpendicular to $\boldsymbol{z}$, e.g. $\boldsymbol{B}_0 = B_0\boldsymbol{x}$. Figure 6 shows the probability of finding a Zeeman qubit, in a $^{88}\text{Sr}^+$ ion,
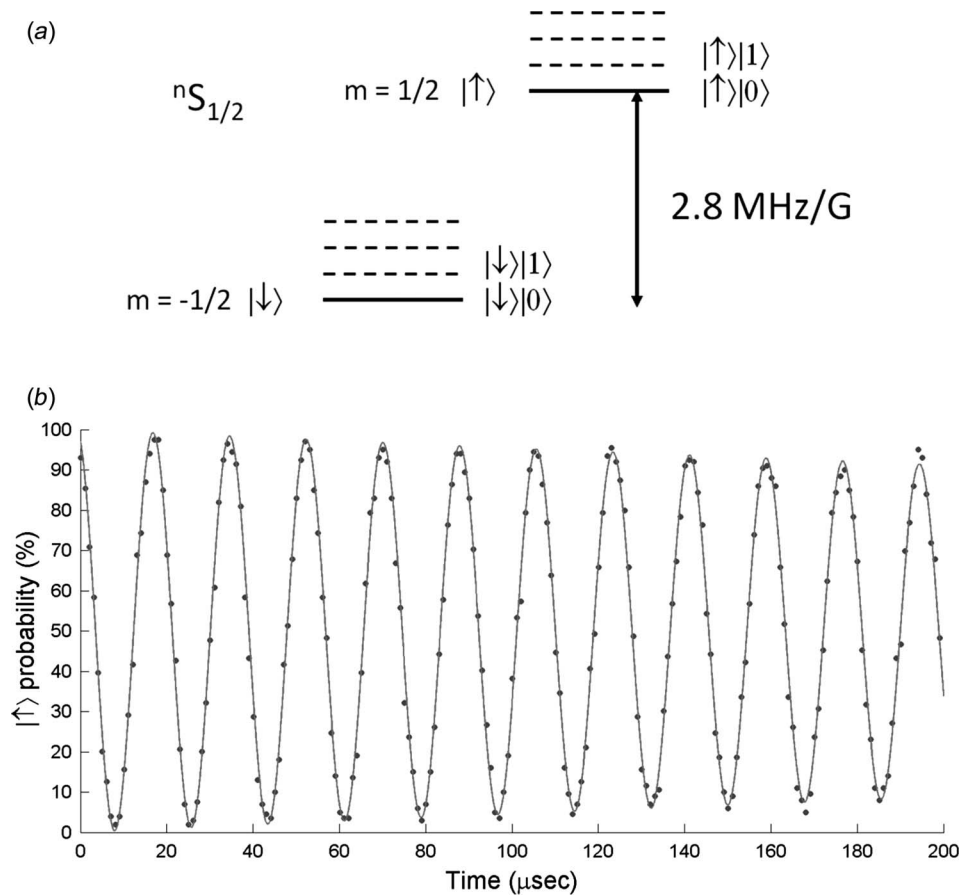

Figure 6.   Magnetic dipole coupling between the two states of a Zeeman qubit in a single trapped $^{88}\text{Sr}^+$ ion. (*a*) A diagram of the Zeeman qubit levels. (*b*) A Rabi-nutation curve. The probability of finding the ion-qubit in the $|\uparrow\rangle$ state oscillates vs. time.

oscillating versus time, due to magnetic-dipole coupling. Since for different ion qubit choices and quantisation magnetic field magnitudes the qubit separation frequency varies between a few MHz and a few GHz, the wavelength of B_0, $\lambda = 1/|k|$ will vary between 0.01 and 1000 m, where the typical x_0 is between 10 and 100 nm. The Lamb–Dicke parameter in this case will be negligibly small, resulting in a carrier Rabi frequency that is almost nearly independent of the ion motion. The disadvantage is that sideband transitions cannot be efficiently driven. Another disadvantage is that this way single-ion qubit addressing is impossible. The fidelity of magnetically driven single-qubit gates is mainly limited by the

amplitude and phase noise of the magnetic RF field at the position of the ion.

3.2. *Two-photon Raman coupling*

Two-photon Raman transitions employ a laser as an optical 'carrier' of the RF qubit separation frequency. In this scheme, photons are coherently transferred between two optical modes with frequencies that are separated by $\omega_0 + s\omega_m$ as illustrated in Figure 7. The laser frequencies are off-resonance, by a detuning Δ_i, with optically allowed transitions from the qubit levels to several excited levels, e_i. With the qubit choices mentioned above, e_i are typically the different states in
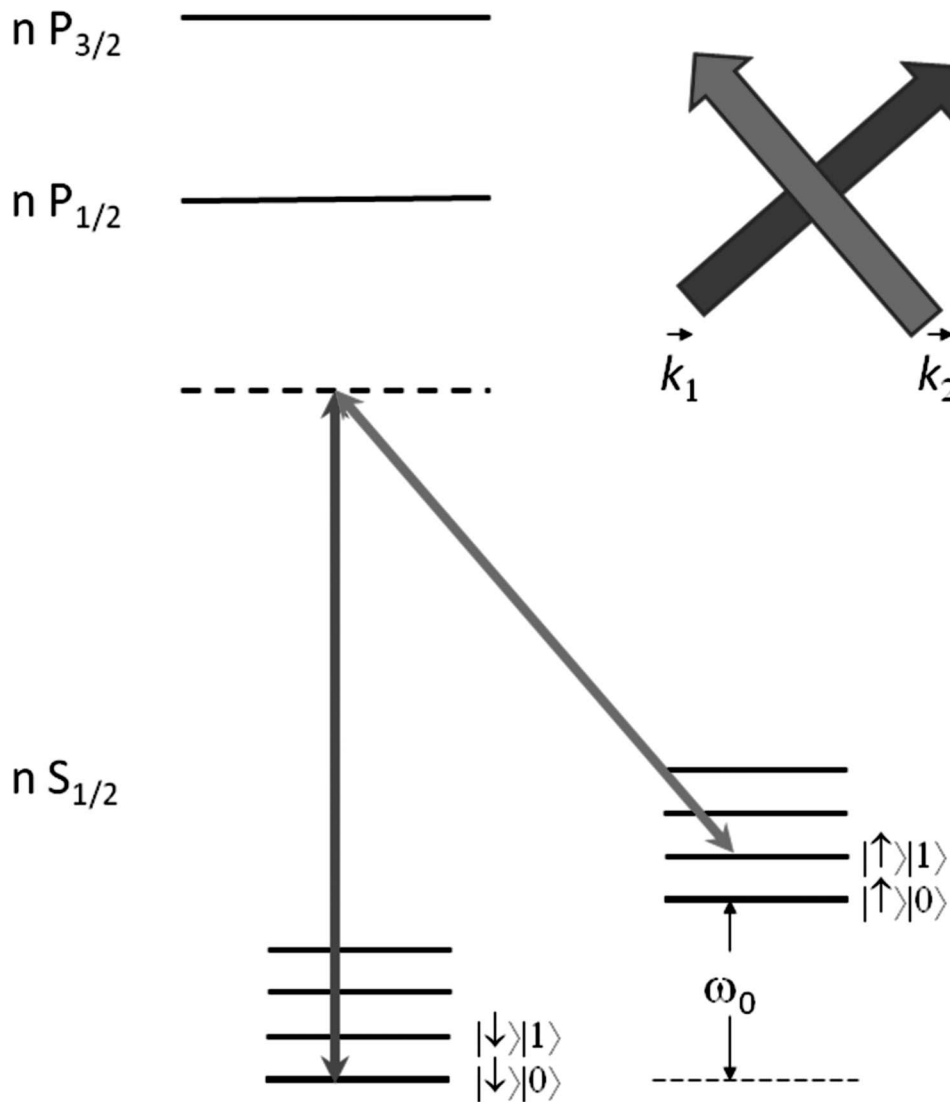
Figure 7. A diagram showing Raman coupling. The Raman beams are detuned from transitions to excited states and the difference in energy between the two beams has to match the energy separation between the two qubit states. In order to excite ion motion, the two Raman beams cannot be co-propagating. A common choice is for the beams to cross at right angle with the difference in their wave-vectors parallel to the trap axis, as shown in the figure.

the $P_{1/2}$ and $P_{3/2}$ levels. Thus, the electric fields of the two Raman modes can be written as

$$\boldsymbol{E}_{r/b} = \varepsilon_{r/b} E_{r/b} \cos(\boldsymbol{k}_{r/b} \cdot \hat{x} - \omega_{r/b} t + \phi_{r/b}), \qquad (19)$$

where red and blue (r/b) correspond to the lower and higher frequency fields, respectively, and ε is a unit vector in the field polarisation direction. To fully solve for the ion evolution, the amplitudes associated with the multiple levels involved have to be calculated. However, when the detuning is significantly larger than the coupling strength, the amplitude associated with the optically excited states, e_i, reduces as $1/\Delta_i$ and oscillates at two time scales, Δ_i, and a slow time scale that adiabatically follows the ground-state amplitudes. It is thus possible to 'adiabatically eliminate' the amplitudes of the e_i states and write the equations of motion only in terms of the ground-state amplitudes and their derivatives. The problem thus reduces to an effective two-level problem involving only the qubit levels. The effective Rabi frequency here is

$$\Omega_0 = \frac{E_r E_b}{4\hbar^2} \sum_i \frac{\langle \uparrow | \hat{d} \cdot \varepsilon_r | e_i \rangle \langle e_i | \hat{d} \cdot \varepsilon_b | \downarrow \rangle}{\Delta_i}. \qquad (20)$$

The time-dependent potential would then reduce to the form of Equation (4), with $\phi = \phi_b - \phi_r$ and $\boldsymbol{k} = \boldsymbol{k}_b - \boldsymbol{k}_r$. The carrier Hamiltonian in the RWA will be

$$\Omega_0 = \hat{H}_{\text{int}} = \frac{\hbar \Omega_0}{2} D_{n,n}(\hat{\sigma}_+ \exp(i\phi) + \hat{\sigma}_- \exp(-i\phi)) + (\Delta_\uparrow - \Delta_\downarrow)\hat{\sigma}_z. \qquad (21)$$

The first term on the rhs is identical to Equation (10). The second term on the rhs is due to the difference in the qubit levels' light shifts induced by the off-resonance Raman beams,

$$\Delta_{\downarrow/\uparrow} = \frac{|E_r|^2}{4\hbar^2} \sum_i \frac{|\langle \downarrow / \uparrow | \hat{d} \cdot \varepsilon_r | e_i \rangle|^2}{\Delta_{i,r}} + \frac{|E_b|^2}{4\hbar^2} \sum_i \frac{|\langle \downarrow / \uparrow | \hat{d} \cdot \varepsilon_b | e_i \rangle|^2}{\Delta_{i,b}}. \qquad (22)$$

The differential light shift can be tuned to zero by carefully choosing the beam polarisation and detuning.

The Lamb–Dicke parameter and therefore the ability to impart momentum and the sensitivity of the Rabi frequency to the ions' motion depends on the angle between the Raman beams. In order to efficiently drive sideband transitions, the angle between the Raman beams needs to be as large as possible and the difference in their wave vector should be such that $\boldsymbol{k}$ has a maximal projection along the trap axis. For the

purpose of driving single qubit rotations it is desirable to avoid changes in the Rabi frequency owing to ion motion and therefore often a co-propagating Raman beam configuration is chosen. Raman beams can be focused to a size limited by the (optical) diffraction limit, typically of the order of a wavelength, and therefore single-ion qubit addressing is in principle possible.

Similarly to the magnetic dipole transition case, errors are caused by classical noises. Laser intensity noise and beam pointing fluctuations result in noise in the Rabi frequency. Phase and frequency noise between the Raman frequency difference and the ion qubit frequency separation also reduces the gate's fidelity. However, in this case, in addition to classical noises, the quantum nature of light will further contribute to the gate error [56]. For laser beams the effect of quantum noise on the interaction with an atom is attributed to spontaneous scattering of photons. Ground-state coherence is only affected by Raman spontaneous scattering events in which a population is transferred between different ground-state levels [57], or when the scattering amplitude from the two qubit states are different [58]. The spontaneous Raman scattering probability during a single qubit gate contributes to the gate error. This contribution reduces for larger Δ_i values.

3.3. Optical quadrupole coupling

Optical qubits are manipulated with optical fields. Consider an optical ion qubit encoded in superpositions of the $|S_{1/2}, m\rangle$ and $|D_{5/2}, m'\rangle$ states. Since the two qubit states have the same parity, it is only electric quadrupole transitions, which require an electric field gradient across the ion, which couple the two levels. Given an optical electric field,

$$\boldsymbol{E} = \varepsilon E_0 \cos(\boldsymbol{k} \cdot \hat{x} - \omega_0 t + \phi) \qquad (23)$$

the electric quadrupole Rabi frequency is given by

$$\Omega_0 = \frac{e E_0}{2\hbar} \langle S_{1/2}, m | (\varepsilon \cdot \boldsymbol{r})(\boldsymbol{k} \cdot \boldsymbol{r}) | D_{5/2}, m' \rangle. \qquad (24)$$

Figure 8 shows the response spectrum of an optical qubit in a single $^{88}Sr^+$ ion to a narrow line width laser scanning across its transition frequency. Red and blue side-bands are apparent on both sides of the carrier transition.

Unlike two-photon Raman transitions, here the Lamb–Dicke parameter cannot be tuned to zero. Errors in optical quadrupole single qubit gates will result from classical noises in the intensity and frequency of the driving laser, and in addition, from
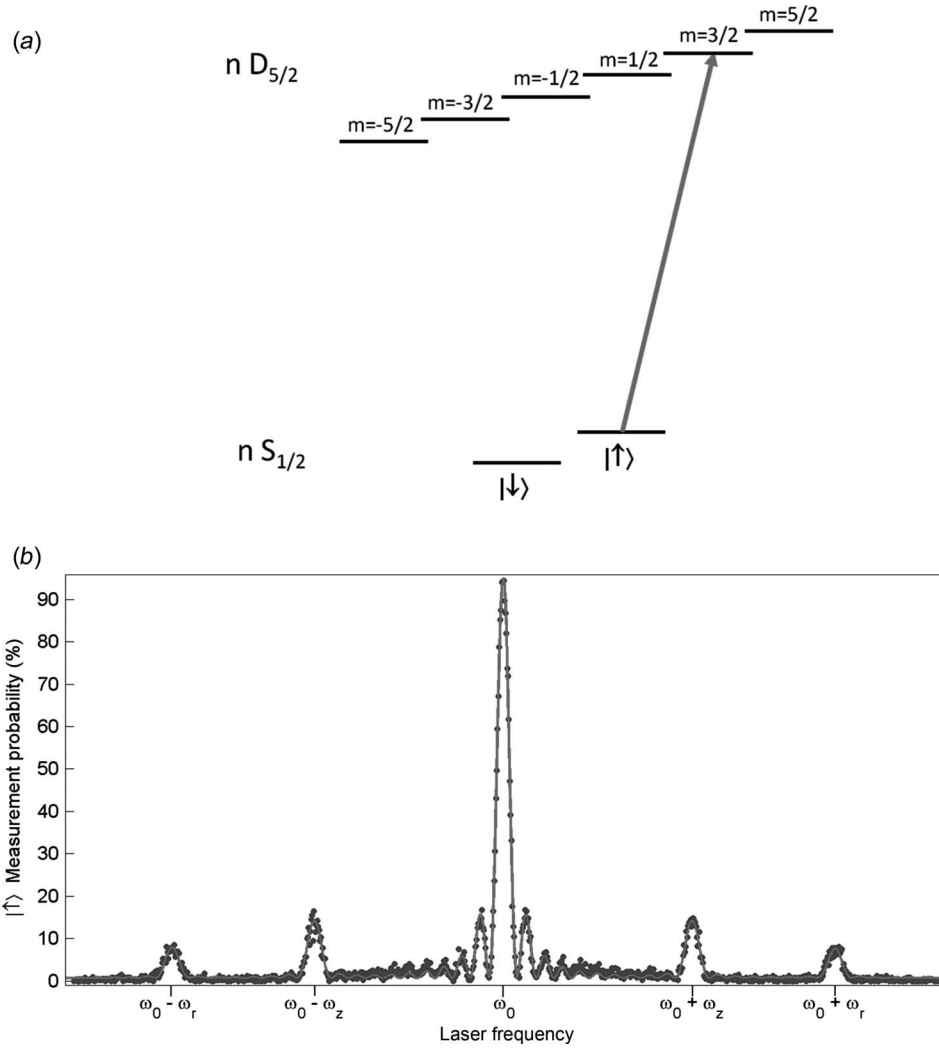
Figure 8. Optical electric–quadrupole coupling between the two states of an optical qubit in a single trapped ^{88}Sr$^+$ion. (*a*) A diagram of the optical qubit levels. (*b*) A spectral response of the ion to the laser frequency. On both sides of the transition carrier are red and blue sidebands corresponding to emission and absorption of longitudinal (z) or radial (r) quanta of motion.

a thermal component in the ions' motion. Another error results from the finite probability of the $D_{5/2}$ level to decay during the gate. However, since the lifetime of the D levels is typically $\simeq 1$ s and much larger than the gate time, this error is typically small.

4. Two-qubit gates

Thus far, we considered only single-qubit rotations. In addition to single-qubit gates, the standard universal gate set includes CNOT entangling operations. CNOT gates rotate the state of a target qubit around the *x*-axis by $180°$, depending on the logical state of a second, control, qubit. Lexicographically ordered, a general two-qubit state is written as the four vector

$$\alpha| \uparrow\uparrow\rangle + \beta| \uparrow\downarrow\rangle + \gamma| \downarrow\uparrow\rangle + \delta| \downarrow\downarrow\rangle = \begin{bmatrix} \alpha \\ \beta \\ \gamma \\ \delta \end{bmatrix}. \qquad (25)$$

The CNOT operation is then represented by the matrix

$$\begin{bmatrix} 1 & 0 & 0 & 0 \\ 0 & 1 & 0 & 0 \\ 0 & 0 & 0 & 1 \\ 0 & 0 & 1 & 0 \end{bmatrix} \begin{bmatrix} \alpha \\ \beta \\ \gamma \\ \delta \end{bmatrix} = \begin{bmatrix} \alpha \\ \beta \\ \delta \\ \gamma \end{bmatrix}. \qquad (26)$$

Since the roles of the target and control qubits are different, implementing this gate on an array of trapped-ion qubits requires a physical operation that

can distinguish between the two. An entangling operation that is symmetric with respect to both ions, appears to be an easier operation to implement. Rotating the target qubit by a Hadamard rotation, which up to a global phase can be composed from two consecutive rotations $\hat{H} = \exp{(i\pi/2)}\hat{R}(0, 0, \pi)\hat{R}(0, \pi/2, \pi/2)$, both before and after the gate, we obtain the operation

$$
[\hat{I}_1 \otimes \hat{H}_2]
\begin{bmatrix}
1 & 0 & 0 & 0 \\
0 & 1 & 0 & 0 \\
0 & 0 & 0 & 1 \\
0 & 0 & 1 & 0
\end{bmatrix}
[\hat{I}_1 \otimes \hat{H}_2] =
\begin{bmatrix}
1 & 0 & 0 & 0 \\
0 & 1 & 0 & 0 \\
0 & 0 & 1 & 0 \\
0 & 0 & 0 & -1
\end{bmatrix}.
\tag{27}
$$

Here, a π phase shift is imprinted on the $|\downarrow\downarrow\rangle$ state with respect to the three other collective spin states. Note that since this gate and the CNOT are connected via single-qubit rotations, they are equivalent in terms of a universal gate set. A subsequent $\pi/2$ rotation of both qubits around the z-axis yields

$$
\hat{R}_1(\pi/2, 0, \pi/2) \otimes \hat{R}_2(\pi/2, 0, \pi/2)
\begin{bmatrix}
1 & 0 & 0 & 0 \\
0 & 1 & 0 & 0 \\
0 & 0 & 1 & 0 \\
0 & 0 & 0 & -1
\end{bmatrix}
$$

$$
= \exp{(-i\pi/2)}
\begin{bmatrix}
1 & 0 & 0 & 0 \\
0 & i & 0 & 0 \\
0 & 0 & i & 0 \\
0 & 0 & 0 & 1
\end{bmatrix}.
\tag{28}
$$

Here, a $\pi/2$ phase is imprinted on anti-parallel spin states with respect to parallel spin states.

Both examples above are entangling operations that rely on imprinting a phase on certain collective spin states. It is important to emphasise that whether a certain entangling operation is a phase gate or not depends on the choice of basis in which it is presented. As an example, the last operation, written in the x basis is,

$$
[\hat{R}_1(0, \pi/2, \pi/2) \otimes \hat{R}_2(0, \pi/2, \pi/2)]
\begin{bmatrix}
1 & 0 & 0 & 0 \\
0 & i & 0 & 0 \\
0 & 0 & i & 0 \\
0 & 0 & 0 & 1
\end{bmatrix}
$$

$$
[\hat{R}_1(0, \pi/2, -\pi/2) \otimes \hat{R}_2(0, \pi/2, -\pi/2)]
$$

$$
= \frac{\exp{(i\pi/4)}}{2^{1/2}}
\begin{bmatrix}
1 & 0 & 0 & -i \\
0 & 1 & -i & 0 \\
0 & -i & 1 & 0 \\
-i & 0 & 0 & 1
\end{bmatrix}
\equiv \hat{U},
\tag{29}
$$

a collective spin flip operation,

$$
\hat{U}|\downarrow\downarrow\rangle = \frac{\exp{(-i\pi/4)}}{2^{1/2}}(|\downarrow\downarrow\rangle + i|\uparrow\uparrow\rangle),
\tag{30}
$$

$$
\hat{U}^2|\downarrow\downarrow\rangle = |\uparrow\uparrow\rangle.
\tag{31}
$$

In fact, most of the proposed implementations of an entangling gate for trapped-ion qubits can be thought of as a phase gate in one basis and a collective spin-flip operation in another.

4.1. Quantum phases in cyclic motion

Entangling phase gates change certain two-qubit collective spin states only by phase factor multiplication. One of those collective spin states undergoes cyclic evolution during the gate, at the end of which, it returns to its initial state with an acquired phase. The phase factors that accompany the cyclic evolution of a quantum state were first studied by Berry for adiabatic state evolution [59] and later by Aharonov and Anandan for the general case [60]. Following [60], let us consider a general quantum state undergoing a cyclic evolution with a period τ,

$$
|\Psi(\tau)\rangle = \exp{(i\phi)}|\Psi(0)\rangle.
\tag{32}
$$

The state evolves according to the time-dependent Schrödinger equation,

$$
\hat{H}(t)|\Psi(t)\rangle = i\hbar(\mathrm{d}/\mathrm{d}t)|\Psi(t)\rangle.
\tag{33}
$$

We define the 'bare' state,

$$
|\Phi(t)\rangle = \exp{[-if(t)]}|\Psi(t)\rangle,
\tag{34}
$$

such that $f(\tau) - f(o) = \phi$. We can now write a differential equation for f,

$$
\frac{\mathrm{d}f}{\mathrm{d}t} = -\frac{1}{\hbar}\langle\Psi(t)|\hat{H}(t)|\Psi(t)\rangle + i\langle\Phi(t)\Big|\frac{\mathrm{d}}{\mathrm{d}t}\Big|\Phi(t)\rangle.
\tag{35}
$$

The phase accumulated by $|\Psi\rangle$ at time τ is given by integrating Equation (35),

$$
\phi = -\frac{1}{\hbar}\int_0^\tau \langle\Psi(t)|\hat{H}(t)|\Psi(t)\rangle\mathrm{d}t
$$
$$
+ i\int_0^\tau \langle\Phi(t)\Big|\frac{\mathrm{d}}{\mathrm{d}t}\Big|\Phi(t)\rangle\mathrm{d}t \equiv \phi_\mathrm{D} + \gamma.
\tag{36}
$$

There are two different contributions to the total phase. The first term on the rhs in Equation (36) is ϕ_D, the dynamic phase, i.e. the time integration of the energy expectation value divided by $\hbar$. The second term

on the rhs is the geometric part of the phase, γ. This part is independent of the exact Hamiltonian under which the state evolves but rather on its evolution path in parameter space. Assuming that at every time instance the wavefunction can be mapped onto a parameter space α, $|\Phi(t)\rangle \equiv |\Phi_\alpha\rangle$, then γ can be written as an integral along a closed α-contour,

$$\gamma = i \int_0^\tau \left\langle \Phi(t) \left| \frac{d}{dt} \right| \Phi(t) \right\rangle dt = i \oint_c \langle \Phi_\alpha | \nabla_\alpha | \Phi_\alpha \rangle \cdot d\alpha. \tag{37}$$

To illustrate the geometric origin of γ, consider a wavefunction evolving around the closed contour in parameter space, as shown in Figure 9. The infinitesimal phase difference, $\Delta\gamma$ between $|\Phi_\alpha\rangle$ and $|\Phi_{\alpha + \Delta\alpha}\rangle$ is defined as

$$\exp(-i\Delta\gamma) = \frac{\langle \Phi_\alpha | \Phi_{\alpha+\Delta\alpha} \rangle}{|\langle \Phi_\alpha | \Phi_{\alpha+\Delta\alpha} \rangle|}. \tag{38}$$

Taking the log of both sides of Equation (38) yields

$$-i\Delta\gamma \simeq \langle \Phi_\alpha | \nabla_\alpha | \Phi_\alpha \rangle \cdot d\alpha. \tag{39}$$

The geometric phase is thus calculated by integrating Equation (39) around the α-contour yielding Equation (37). By defining the vector potential

$$\boldsymbol{A}_\alpha = i\langle \phi_\alpha | \nabla_\alpha | \phi_\alpha \rangle, \tag{40}$$

we can write an effective 'magnetic field',

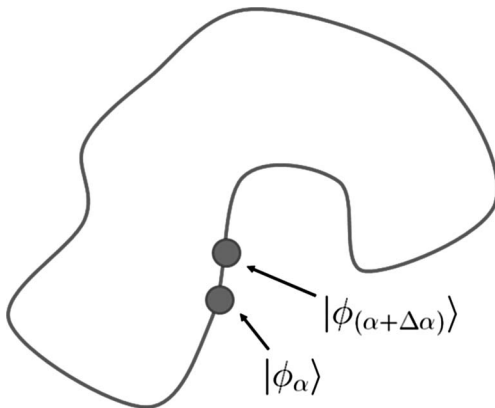$$\boldsymbol{B}_\alpha = \nabla \times \boldsymbol{A}_\alpha. \tag{41}$$

Figure 9. A wavefunction evolving around a closed contour in parameter space. The two circles represent the wavefunction at α and $\alpha + \Delta\alpha$.

Using Stokes theorem we then express the geometric phase as the effective magnetic field flux through the parameter space area, S,

$$\gamma = -\int\int_S \boldsymbol{B} \cdot \boldsymbol{n} \, dS. \tag{42}$$

Here $\boldsymbol{n}$ is the unit vector normal to S. The encirclement of a finite area in parameter space is therefore a necessary condition for accumulating a geometrical phase in cyclic motion.

An ion qubit is a (pseudo-) spin connected to a harmonic oscillator. A phase gate such as (28) can be implemented by acquiring either a dynamic or a geometric phase or both, during a cyclic motion either in spin configuration space or in the h.o. phase space. Cirac and Zoller's seminal 1995 proposal for an entangling gate with trapped-ion qubits [14] implements a phase gate where the phase is geometric and the cyclic motion is in spin configuration space. A later proposal by the same authors uses a dynamic phase acquired during a cyclic motion in phase space [61]. In the following section we will concentrate on a class of gates, initially proposed by Sørensen and Mølmer [15] and independently by Milburn and co-authors [16], which uses spin-dependent forces to acquire a sum of geometric and dynamic phases during a cyclic motion in h.o. phase space.

4.2. Driven harmonic oscillator

A classical harmonic oscillator evolves periodically in phase space under the influence of a force, $F(t) = F_0 \cos(\omega t)$, oscillating at a frequency slightly off-resonance from its harmonic frequency, $\omega = \omega_m - \delta$. Starting at rest, $x(t = 0) = p(t = 0) = 0$, the position and momentum of the oscillator at subsequent times are given by,

$$x(t) = \frac{F_0/m}{\omega^2 - \omega_m^2} [\cos(\omega t) - \cos(\omega_m t)] \tag{43}$$

$$p(t) = \frac{F_0}{\omega^2 - \omega_m^2} [\omega_m \sin(\omega_m t) - \omega \sin(\omega t)]. \tag{44}$$

Initially the driving force increases the oscillation amplitude until, at time $t = \pi/\delta$, the force and the oscillator are out of phase. From this time onward the force dampens the oscillator until, at time $t = 2\pi/\delta$, the oscillator returns to its initial state. To make an analogy with the quantum case, we normalise the h.o. position by $2x_0$ and the momentum by $p_0 \equiv \hbar/x_0$ and move to a frame rotating at the oscillator frequency. Neglecting terms that are proportional to δ/ω_m we arrive at

$$x'(t) = \frac{x(t)}{2x_0} \cos(\omega_m t) - \frac{p(t)}{p_0} \sin(\omega_m t)$$
$$\equiv \frac{F_0 x_0}{2\hbar\delta}[1 - \cos(\delta t)], \quad (45)$$

$$p'(t) = \frac{x(t)}{2x_0} \sin(\omega_m t) + \frac{p(t)}{p_0} \cos(\omega_m t)$$
$$\equiv \frac{F_0 x_0}{2\hbar\delta}[\sin(\delta t)]. \quad (46)$$

We define the complex function $\alpha(t) = x'(t) + ip'(t)$. The h.o. oscillator motion in the complex plane is along the curve

$$\alpha(t) = \frac{F_0 x_0}{2\hbar\delta}[1 - \exp(i\delta t)]. \quad (47)$$

The h.o. therefore periodically evolves around a circle in the complex plane, the area of which is

$$S = \pi\left[\frac{F_0 x_0}{2\hbar\delta}\right]^2. \quad (48)$$

We now turn to solving the quantum, driven, harmonic oscillator. The quantum Hamiltonian of a driven h.o. is

$$H = \hbar\omega_m(\hat{a}^\dagger\hat{a} + 1/2) + F(t)\hat{x} \equiv H_0 + V(t). \quad (49)$$

Note that here we assume that the force is spatially uniform and therefore it does not vary across the h.o. wavefunction. Moving to the interaction representation and using the RWA we write $i\hbar(d/dt)|\Psi\rangle_I = V_I|\Psi\rangle_I$, with

$$V_I = \frac{F_0 x_0}{2}\left(\hat{a}^\dagger\exp(i\delta t) + \hat{a}\exp(-i\delta t)\right). \quad (50)$$

V_I does not commute with itself at different times; however, for a short enough Δt, we can still write

$$|\Psi(t + \Delta t)\rangle_I = \exp\left(-\frac{i}{\hbar}V_I\Delta t\right)|\Psi(t)\rangle_I$$
$$= \exp\left[(\Delta\alpha\hat{a}^\dagger + \Delta\alpha^\star\hat{a})\right]|\Psi(t)\rangle_I$$
$$\equiv \hat{D}(\Delta\alpha)|\Psi(t)\rangle_I, \quad (51)$$

where $\hat{D}(\Delta\alpha)$ is the displacement operator,

$$\hat{D}(\alpha)|0\rangle = |\alpha\rangle = \exp\left(-\frac{1}{2}|\alpha|^2\right)\sum_{n=0}^{\infty}\frac{\alpha^n}{(n!)^{1/2}}|n\rangle. \quad (52)$$

When operating on the h.o. ground-state the displacement operator forms coherent states of motion. Here the infinitesimal displacement is

$$\Delta\alpha(t) = -\frac{i}{2\hbar}F_0 x_0 \exp(i\delta t)\Delta t \equiv [\Delta x/2x_0 + ip/p_0].$$
$$(53)$$

The real and imaginary part of the displacement can be identified with its position and momentum parts, respectively. To add two infinitesimal displacements, we use the Baker–Hausdorff formula,

$$\exp(\hat{A})\exp(\hat{B}) = \exp(\hat{A} + \hat{B})\exp\left(\frac{1}{2}[\hat{A}, \hat{B}]\right), \quad (54)$$

for operators $\hat{A}$ and $\hat{B}$ that commute with their commutator, $[\hat{A}, [\hat{A}, \hat{B}]] = [\hat{B}, [\hat{A}, \hat{B}]] = 0$. We thus get

$$\hat{D}(\alpha)\hat{D}(\beta) = \hat{D}(\alpha + \beta)\exp[i\,\text{Im}(\alpha\beta^\star)]. \quad (55)$$

The displacement operator can accordingly be re-written as

$$\hat{U}(t = 0, t) = \hat{D}\left(\sum_{i=1}^{N}\Delta\alpha_i\right)$$
$$\exp\left\{i\,\text{Im}\left[\sum_{j=2}^{N}\Delta\alpha_j\left(\sum_{k=1}^{j-1}\Delta\alpha_k\right)^*\right]\right\}$$
$$= \hat{D}(\alpha)\exp\left(i\,\text{Im}\oint \alpha * d\alpha\right), \quad (56)$$

with, $\alpha = \sum_{i=1}^{N}\Delta\alpha_i$. The total displacement at time, t, is therefore,

$$\alpha(t) = \int_o^t \Delta\alpha(t)dt = -\frac{i}{2\hbar}\int_o^t F_0 x_0 \exp(i\delta t')dt'$$
$$= \frac{F_0 x_0}{2\hbar\delta}(1 - \exp(i\delta t)). \quad (57)$$

The quantum wavefunction and the classical h.o. therefore follow an *identical* trajectory in phase space, illustrated in Figure 10. As in the classical case, after time $\tau_g = 2\pi/\delta$, the h.o. wavefunction returns to its initial state.

The total phase that is accumulated by the end of the gate is

$$\phi = \text{Im}\oint \alpha^\star d\alpha = \frac{\pi}{2}\left(\frac{F_0 x_0}{\hbar\delta}\right)^2. \quad (58)$$

To implement the phase gate (28), the force magnitude and detuning are adjusted such that $\phi = \pi/2$. Comparing the phase to the area encircled in phase space during the gate, Equation (48), we obtain
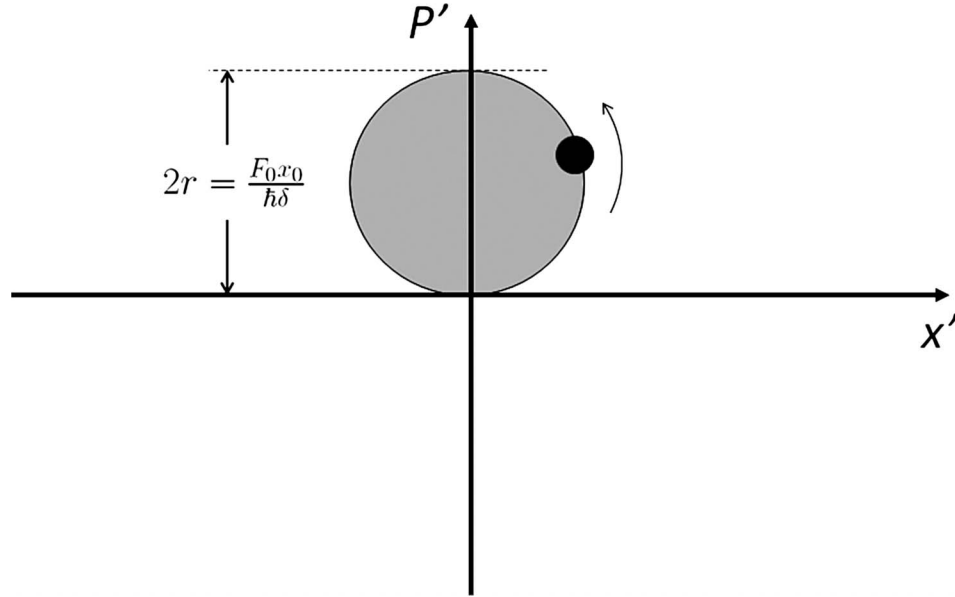
$$\gamma = 2S. \quad (59)$$

Figure 10. An illustration of the quantum driven harmonic-oscillator wavefunction trajectory through phase-space. The oscillator is starting from the ground-state and is off-resonantly driven with a periodic force with amplitude F_0. The area that the oscillator is circulating in phase space is equal to $S = \pi [F_0 x_0 / 2\hbar\delta]^2$.

A proportionality between the phase accumulated per cycle and the area encircled by the wavefunction in phase space suggests that the phase has a geometric origin.

To make the connection with Equation (36) we calculate the dynamic and geometric contributions to ϕ. The dynamic phase is simply

$$
\begin{aligned}
\phi_{\mathrm{D}} &= -\frac{1}{\hbar} \int_0^{\tau_{\mathrm{g}}} \langle \alpha(t) | \hat{V}_I(t) | \alpha(t) \rangle \, \mathrm{d}t \\
&= \frac{F_0 x_0}{2\hbar} \int_0^{2\pi/\delta} (\alpha^\star \exp(\mathrm{i}\delta t) + \alpha^{-\mathrm{i}\delta t}) \\
&= \pi \left(\frac{F_0 x_0}{\hbar\delta} \right)^2 = 2\phi.
\end{aligned}
\tag{60}
$$

The geometric part of the phase is

$$
\gamma = \mathrm{i} \oint_c \langle \alpha | \nabla | \alpha \rangle \cdot \mathrm{d}\alpha.
\tag{61}
$$

Here phase space is the parameter space (a complex plane) and the wavefunction trajectory is parameterised by the complex displacement α. We evaluate the integrand along the wavefunction path by

$$
\langle \alpha | \nabla | \alpha \rangle \cdot \mathrm{d}\alpha = \langle \alpha | \alpha + \Delta\alpha \rangle - 1.
\tag{62}
$$

Coherent states are an over-complete basis of wavefunctions and are therefore not mutually orthogonal. The overlap between two coherent states α and β is

$$
\langle \alpha | \beta \rangle = \exp\left[-\frac{1}{2}(|\alpha|^2 + |\beta|^2) + \alpha^\star\beta \right].
\tag{63}
$$

We therefore arrive at

$$
\langle \alpha | \alpha + \Delta\alpha \rangle - 1 \simeq \frac{1}{2}(\alpha^\star \Delta\alpha - \alpha\Delta\alpha^\star) = \mathrm{i}\,\mathrm{Im}(\alpha^\star \Delta\alpha),
\tag{64}
$$

leading to the geometric phase

$$
\gamma = -\mathrm{Im} \oint \alpha^\star \, \mathrm{d}\alpha = -\phi.
\tag{65}
$$

The total phase acquired during the gate is consequently the sum of partially cancelling dynamic and geometric contributions. Although of different origin, the geometric and dynamic parts of the phase are proportional to each other. The total phase, therefore, is also proportional to the geometric phase and accordingly, to the area encircled in phase space [62]. The fact that ϕ depends on the wavefunction path in phase-space rather than on dynamic properties of the gate Hamiltonian contributes to the phase gate robustness against noise.

Following Equation (40) we can define a vector potential,

$$A = i\langle\alpha|\nabla|\alpha\rangle = [-\mathrm{Im}(\alpha), +\mathrm{Re}(\alpha), 0]. \qquad (66)$$

The effective magnetic field (as in Equation (41)) is then perpendicular to the complex plane, i.e. $\boldsymbol{B} = B_z\boldsymbol{z}$ and constant,

$$B_z = \frac{\partial\mathrm{Re}(\alpha)}{\partial\mathrm{Re}(\alpha)} + \frac{\partial\mathrm{Im}(\alpha)}{\partial\mathrm{Im}(\alpha)} = 2. \qquad (67)$$

By using the Stokes theorem, Equation (42), we again find that the geometric phase equals minus twice the phase-space area encircled, as in Equations (59) and (65). The motion of the h.o. wavefunction in phase-space (in the interaction representation) is therefore analogous to the motion of a charged particle in a uniform magnetic field. The acquired geometric phase is therefore analogous to the Aharonov–Bohm phase.

4.3. Spin-dependent forces

Acquiring a phase is not sufficient for realising a two-qubit phase gate such as in Equation (28). The phase acquired and therefore also the wavefunction trajectory through phase-space have to be dependent on the collective two-qubit spin state. To this end, spin-dependent forces have to be used.

Since light couples differently to different spin states, it can be used to apply spin-dependent forces on trapped-ion qubits. Spin-dependent forces can be applied to Zeeman or hyperfine ion qubits by using the differential light shift, Equation (22). Here, a spatial variation in the light shift induces different forces on ions in different collective spin states. Ions in a collective spin superposition move along position-momentum paths that are entangled with the different spin states. Since the force evolution is cyclic, spin and motion are disentangled at the end of the gate. Here, since the different collective spin states are eigenstates of $\hat{\sigma}_z \otimes \hat{\sigma}_z$, the gate is referred to as a σ_z gate.

It is somewhat less trivial using the light shift, due to coupling to a third level, to apply spin-dependent forces to an optical ion qubit. This is because for a given transition wavelength, when one of the qubit levels is connected to a third level, only that level will be light shifted. Forces on the two ion qubits will only depend on one of the qubit states. Another example of an ion qubit on which such σ_z gates fail are 'magnetic field insensitive' qubits. Here, since the magnetic field couples primarily to the electron spin, and to a far lesser degree to the nuclear spin, 'magnetic field insensitive' qubits have equal amplitudes of different electron spin contributions to the two qubit states [63]. Light also couples primarily to the electron spin and therefore the difference in light shifts is very small and is mainly due to the small difference in detuning

between both qubit states. These small differential light shifts are insufficient to efficiently drive an entangling gate. Entangling phase gates on the two ion qubits mentioned above are possible, however, when differential forces are applied on spin states that lie on the Bloch sphere equatorial plane. In the measurement basis, the action of these gates is similar to Equation (30). Since this gate is a phase gate in the basis of eigenstates of $\hat{\sigma}_\phi \otimes \hat{\sigma}_\phi$, where $\hat{\sigma}_\phi = \cos\phi\hat{\sigma}_x + \sin\phi\hat{\sigma}_y$, i.e. ϕ is the angle form the positive x-axis, the gate is often referred to as a σ_ϕ gate.

4.4. σ_z gates

In the case of magnetic field-sensitive Zeeman or hyperfine qubits, σ_z gates can be driven with a pair of beams similar to the single-qubit Raman gate case, Equation (20). Here, however, the difference in frequency between the beams is far from the qubit transition frequency, ω_0, and is close to resonance with the trap motional frequency, $\omega_b - \omega_r = \omega_m + \delta$. In the RWA, no terms are resonant and therefore no direct coupling between the two qubit levels occurs. Instead, the only effect of the light field is to shift the two qubit levels by $\Delta_{\uparrow/\downarrow}$, given in Equation (22).

To form a spatially varying potential, the two beams are crossed such that the vector difference of their wavevectors, $\Delta k = k_b - k_r$, is parallel to the axial direction of the trap. By choosing beam polarisations mutually perpendicular and with a magnetic field direction that is perpendicular to both one obtains a local polarisation of the light field that varies periodically between right circular, linear, left circular, a linear polarisation perpendicular to the previous, and back to right circular, over a period of $2\pi/\Delta k$. This configuration is often referred to as the lin $\perp$ lin configuration, known from Sisyphus cooling. The light potential of each of the qubit levels can hence be written as,

$$\Delta_{\downarrow/\uparrow}(x,t) = \frac{1}{2}(\Delta_{\downarrow/\uparrow,+} + \Delta_{\downarrow/\uparrow,-}) + \frac{1}{2}[\Delta_{\downarrow/\uparrow,+} - \Delta_{\downarrow/\uparrow,-}]$$
$$\cos(\Delta\boldsymbol{k}\cdot\boldsymbol{x} - \Delta\omega t + \Delta\phi). \qquad (68)$$

Here $\Delta_{\downarrow/\uparrow,+}$ and $\Delta_{\downarrow/\uparrow,-}$ are the light shifts of the $\downarrow$ and $\uparrow$ qubit levels owing to the presence of a right and left circularly polarised field, respectively. The force on each of the qubit levels is therefore,

$$F_{\downarrow/\uparrow}(x,t) = -\frac{\mathrm{d}\Delta_{\downarrow/\uparrow}(x,t)}{\mathrm{d}x}$$
$$= \frac{\hbar k}{2}[\Delta_{\downarrow/\uparrow,+} - \Delta_{\downarrow/\uparrow,-}]\cos(\Delta kx - \Delta\omega t + \Delta\phi).$$
$$(69)$$

With two equal-mass ions in the trap, there are two normal modes of motion along the trap longitudinal axis. The centre of mass (CM) mode, where the two ions oscillate in phase, has an angular frequency that equals that of a single ion, $\omega_{\mathrm{cm}} = \omega_{\mathrm{m}}$. The second mode is the 'stretch' (ST) mode, where the two ions oscillate out of phase, has an angular frequency of $\omega_{\mathrm{st}} = 3^{1/2}\omega_{\mathrm{m}}$ [64]. The position operator of each ion can be written as,

$$\hat{x}_i = x_{\mathrm{eq},i} + \frac{x_{\mathrm{cm0}}}{2^{1/2}}(\hat{a}^\dagger_{\mathrm{cm}} + \hat{a}_{\mathrm{cm}}) \pm \frac{x_{\mathrm{st0}}}{2^{1/2}}(\hat{a}^\dagger_{\mathrm{st}} + \hat{a}_{\mathrm{st}}), \quad (70)$$

where $\hat{a}^\dagger_{\mathrm{cm}}$ ($\hat{a}_{\mathrm{cm}}$) and $\hat{a}^\dagger_{\mathrm{st}}$ ($\hat{a}_{\mathrm{st}}$) are the creation (annihilation) operators of the CM and ST modes, respectively. The root mean square of the ground-states' spatial spread of the two normal modes are x_{cm0} and x_{st0}. The $+ (-)$ signs correspond to the ion with a positive (negative) equilibrium x position. This sign change is due to the ions' opposite direction of motion in the ST mode. When exciting the CM mode the total force is the sum of forces on the two ions, and when exciting the ST mode the total force is the difference in forces. The treatment of a driven h.o. above assumes a uniform force. In the Lamb–Dicke regime we neglect the variation of the force (69) over the ions' wavefunction spread, thus neglecting wavefunction squeezing effects during the gate [65]. The force is accordingly considered as uniform with a value given by Equation (69) at the ions' equilibrium position.

4.5. σ_ϕ gates

As discussed in Section 4.3, it is hard to apply spin-dependent forces to certain ion qubit realisations such as optical-qubits or hyperfine clock-transition qubits [63]. It is possible, however, to apply forces that will depend on their superpositions. In particular, it is possible to apply forces that will be equal in magnitude but opposite in direction on the two qubit states: $|+\phi\rangle = 2^{-1/2}(|\uparrow\rangle + \exp(\mathrm{i}\phi)|\downarrow\rangle)$ and $|-\phi\rangle = 2^{-1/2}(|\uparrow\rangle + \exp(-\mathrm{i}\phi)|\downarrow\rangle)$. Here, spin-dependent forces are applied in a basis that lies in the equatorial plane of the initial qubit (ion energy eigenstates) Bloch-sphere. As shown in Equation (30), in the qubit basis this operation will look like a collective spin rotation. This kind of gate was initially proposed by Sørensen and Mølmer [15] and demonstrated both on hyperfine as well as optical qubits [21,66].

5. Summary

In this tutorial we reviewed several of the building blocks necessary for QIP with trapped-ion qubits. We focused on ways by which a universal quantum gate set can be implemented, and in particular on quantum gates which are driven by electro-magnetic fields in the far-field region. Here, in order to impart momentum to a cold ion, optical fields are needed. Use of optical fields requires relatively narrow line-width lasers. Since atomic transitions of ions are typically in the violet to ultraviolet spectral regions, lasers are needed at this wavelength range. The advent of gallium-nitride diode lasers has significantly lowered the cost of near-UV and violet laser systems. In fact, for some ion species considered as quantum information carriers, such as Ca^+ or Sr^+, all the necessary wavelengths for QIP operations are available either directly, or with frequency-doubled, diode laser systems. There are, however, several difficulties and disadvantages in using light fields as control fields for QIP. One difficulty is in integrating light into a large-scale ion-trap architecture [7]. Realistically, all the routing (e.g. with optical fibres) and switching will have to be multiplexed into the trap array structure. This is a non-trivial task and several initial steps have been taken in this direction [67]. Another disadvantage is that, although treated here in a classical fashion, a light field (as well as any other control field) is essentially a quantum field, featuring quantum noise in its operation on a qubit. Quantum noise in the operation of a certain control field will pose a quantum limit to the operation's fidelity. In the operation of light fields on an atom, this error can be thought of as originating from spontaneous scattering of photons during the gate operation [56]. Optical light fields suffer from this type of error to a much larger extent than do control fields in the radio-frequency or microwave frequency range. It is important to note that our review is not at all exhaustive. For example, in the last few years, alternative methods have been suggested, with a few initial demonstrations, in which a universal quantum gate set is performed on trapped-ion qubits using only microwave fields [51]–[55]. Here, momentum transfer to trapped-ions is achieved with strong magnetic field gradients.

As mentioned in the introduction to this tutorial, despite experimental realisation of all the basic building blocks for a trapped-ion quantum computer, there are many different difficulties that must be overcome until a large-scale device is finally realised. One such difficulty lies in the way decoherence, or error, scales as a function of the quantum register size. Without active error-correction, the error probability in a quantum register after a given time would scale exponentially with the register size, thus negating large-scale quantum computing. Fortunately, it has been shown that by using certain error-correction protocols, and given that the error-probability per operation is below a certain threshold, large scale quantum computing is rendered fault-tolerant [68,69].

This means that under these conditions, the error in a quantum computation would be independent of the register size or the number of computational steps. The fault-tolerance threshold is not cast in stone and depends on many parameters such as the exact noise mechanism, the error-correction protocol used, the register architecture and so forth. However, under rather general assumptions, this threshold has been estimated to be in the 10^{-2}–10^{-4} range [70]. In the last few years, a large effort has been directed toward perfecting all the basic operations on trapped-ion qubits, e.g. initialisation, detection, memory error, and one- and two-ion gates, and reducing the error in these operations as much as possible. Currently, typical errors in the gates described above are also in the 10^{-2}–10^{-4} range [21,43,47,71,72], with good prospects for further improvements.

There is a broad consensus, we believe, that a very large gap exists between the QIP capabilities demonstrated so far with trapped-ion qubits, or any other qubit technology for that matter, and realising a large-scale quantum computer. On the other hand, this gap is also widely believed to be purely technological rather than fundamental. If this is the case, with more effort and time, a quantum computer will eventually be realised. Failure to eventually realise a quantum computer will be glamorous because it will indicate a need to modify the laws of quantum mechanics when describing large-scale systems.

Acknowledgements

Notes on contributor

Roee Ozeri received his Ph.D. in experimental Physics from the Weizmann Institute of Science in 2003. After three years as a research fellow at the National Institute of Standards and Technology in Boulder, Colorado, he returned to the Weizmann Institute as a faculty member. Since 2007 he has been a senior researcher at the Weizmann Institute. His current research uses laser-cooled trapped ions to perform experiments in quantum information science and quantum metrology as well as the study of ultra-cold atomic interactions.

References

[1] M.A. Nielsen and I.L. Chuang, *Quantum Information and Quantum Information*, Cambridge University Press, Cambridge, 2000.

[2] E. Schrödinger, *Die gegenwärtige situation in der quantenmechanik*, Die Naturwissenschaften 23 (1935), p. 844.

[3] D.J. Wineland, C. Monroe, W.M. Itano, D. Leibfried, B.E. King, and D.M. Meekhof, *Experimental issues in coherent quantum state manipulation of trapped atomic ions*, J. Res. Nat. Inst. Stand. Tech. 103 (1998), p. 259.

[4] D. Leibfried, R. Blatt, C. Monroe, and D.J. Wineland, *Quantum dynamics of single trapped ions*, Rev. Mod. Phys. 75 (2003), p. 281.

[5] J.P. Home, D. Hanneke, J.D. Jost, J.M. Amini, D. Leibfried, and D.J. Wineland, *Complete methods set for scalable ion trap quantum information processing*, Science 325 (2009), p. 1227.

[6] D. Kielpinski, C. Monroe, and D.J. Wineland, *Architecture for a large-scale ion-trap quantum computer*, Nature 417 (2002), p. 709.

[7] J. Kim and C. Kim, *Integrated optical approach to trapped ion quantum computation*, Quantum Inf. Comput. 9 (2009), p. 181.

[8] D. Deutsch, *Quantum computational networks*, Proc. R. Soc. London Ser. A 425 (1989), p. 73.

[9] A. Barenco, C.H. Bennett, R. Cleve, D.P. DiVincenzo, N. Margolus, P. Shor, T. Sleator, J.A. Smolin, and H. Weinfurter, *Elementary gates for quantum computation*, Phys. Rev. A 52 (1995), p. 3457.

[10] A.Y. Kitaev, *Quantum computations: algorithms and error correction*, Russ. Math. Surv. 52 (1997), p. 1191.

[11] L. Essen and J.V.L. Parry, *An atomic standard of frequency and time interval: a cæsium resonator*, Nature 176 (1955), p. 280.

[12] C. Cohen-Tannoudji, J. Dupont-Roc, and G. Grynberg, *Atom–Photon Interactions*, Wiley, New York, 1998

[13] J.E. Nafe, E.B. Nelson, and I.I. Rabi, *The hyperfine structure of atomic hydrogen and deuterium*, Phys. Rev. 71 (1947), p. 914.

[14] J.I. Cirac and P. Zoller, *Quantum computations with cold trapped ions*, Phys. Rev. Lett. 74 (1995), p. 4091.

[15] A. Sørensen and K. Mølmer, *Quantum computation with ions in thermal motion*, Phys. Rev. Lett. 82 (1999), p. 1971.

[16] G.J. Milburn, S. Schneider, and D.F.V. James, *Ion trap quantum computing with warm ions*, Fortschr. Phys. 48 (2000), p. 801.

[17] J.J. Garcia-Ripoll, P. Zoller, and J.I. Cirac, *Speed optimized two-qubit gates with laser coherent control techniques for ion trap quantum computing*, Phys. Rev. Lett. 91 (2003), 157901.

[18] S.-L. Zhu, C. Monroe, and L.M. Duan, *Trapped ion quantum computation with transverse phonon modes*, Phys. Rev. Lett. 97 (2006), 050505.

[19] K. Kim, C.F. Roos, L. Aolita, H. Häffner, V. Nebendahl, and R. Blatt, *Geometric phase gate on an optical transition for ion trap quantum computation*, Phys. Rev. A 77 (2008), 050303.

[20] D. Liebfried, B. DeMarco, V. Meyer, D. Lucas, M. Barrett, J. Britton, W.M. Itano, B. Jelenkovic, C. Langer, T. Rosenband, and D.J. Wineland, *Experimental demonstration of a robust, high-fidelity geometric two ion-qubit phase gate*, Nature 422 (2003), p. 412.

[21] J. Benhelm, G. Kirchmair, C.F. Roos, and R. Blatt, *Towards fault-tolerant quantum computing with trapped ions*, Nat. Phys. 4 (2008), p. 463.

[22] D.J. Wineland, R.E. Drullinger, and F.L. Walls, *Radiation-pressure cooling of bound resonant absorbers*, Phys. Rev. Lett. 40 (1978), p. 1639.

[23] W.M. Itano, J.C. Bergquist, and D.J. Wineland, *Measurements of the gJ factors of the $6s^2 1/2$ and $6p^2 P1/2$ states in $198Hg^+$*, J. Opt. Soc. Am. B 2 (1985), p. 1392.

[24] J.J. Bollinger, J.S. Wells, D.J. Wineland, and W.M. Itano, *Hyperfine structure of the 2p2P1/2 state in 9Be$^+$*, Phys. Rev. A 31 (1985), p. 2711.

[25] M. Schubert, I. Siemers, and R. Blatt, *Spatially localized optical pumping in Paul traps*, J. Opt. Soc. Am. B 6 (1989), p. 2159.

[26] A.A. Madej and J.D. Sankey, *Single, trapped Sr$^+$ atom: laser cooling and quantum jumps by means of the $4d^2D_{5/2}$–$5s^2S_{1/2}$ transition*, Opt. Lett. 15 (1990), p. 634.

[27] H.A. Klein, A.S. Bell, G.P. Barwood, and P. Gill, *Laser cooling of trapped Yb$^+$*, Appl. Phys. B 50 (1990), p. 13.

[28] T. Gudjons, F. Arbes, M. Benzing, F. Kurth, and G. Werth, *Spatial fluorescence distribution and laser cooling of Ca$^+$ in a Paul trap*, Phys. Scr. T 59 (1995), p. 396.

[29] U. Tanaka, H. Imajo, K. Hayasaka, R. Ohmukai, M. Watanabe, and S. Urabe, *Laser cooling and isotope separation of Cd$^+$ ions confined in a linear Paul trap*, Opt. Lett. 22 (1997), p. 1353.

[30] K. Matsubara, U. Tanaka, H. Imajo, S. Urabe, and M. Watanabe, *Laser cooling and isotope-shift measurement of Zn$^+$ with 202-nm ultraviolet coherent light*, Appl. Phys. B 76 (2003), p. 209.

[31] D.M. Lucas, C.J.S. Donald, J.P. Home, M.J. McDonnell, A. Ramos, D.N. Stacey, J.-P. Stacey, A.M. Steane, and S.C. Webster, *Oxford ion-trap quantum computing project*, Phil. Trans. R. Soc. Lond. A 361 (2003), p. 1401.

[32] D.J. Wineland, C.R. Monroe, W.M. Itano, B.E. King, D. Leibfried, D.M. Meekhof, C.J. Myatt, and C.S. Wood, *Experimental primer on the trapped ion quantum computer*, Fortschr. Phys. 46 (1998), p. 363.

[33] B.B. Blinov, D. Leibfried, C. Monroe, and D.J. Wineland, *Quantum computing with trapped ion hyperfine qubits*, Quantum Inf. Proc. 3 (2004), p. 45.

[34] C. Balzer, A. Braun, T. Hannemann, C. Paape, M. Ettler, W. Neuhauser, and C. Wunderlich, *Electrodynamically trapped Yb$^+$ ions for quantum information processing*, Phys. Rev. A 73 (2006), 041407.

[35] S. Olmschenk, K.C. Younge, D.L. Moehring, D.N. Matsukevich, P. Maunz, and C. Monroe, *Manipulation and detection of a trapped Yb$^+$ hyperfine qubit*, Phys. Rev. A 76 (2007), 052314.

[36] J. Benhelm, G. Kirchmair, C.F. Roos, and R. Blatt, *Experimental quantum-information processing with ^{43}Ca$^+$ ions*, Phys. Rev. A 77 (2008), 062306.

[37] C.J. Foot, *Atomic Physics*, Oxford University Press, Oxford, 2005.

[38] C.E. Langer, *High fidelity quantum information processing with trapped ions*, Ph.D. thesis, University of Colorado, Boulder, 2006.

[39] H.G. Dehmelt, *Proposed 10^{14} Dv < v laser fluorescence spectroscopy on Tl+ mono-ion oscillator II (spontaneous quantum jumps)*, Bull. Am. Phys. Soc. 20 (1975), p. 60.

[40] W.M. Itano, J.C. Bergquist, J.J. Bollinger, J.M. Gilligan, D.J. Heinzen, F.L. Moore, M.G. Raizen, and D.J. Wineland, *Quantum projection noise: Population fluctuations in two-level systems*, Phys. Rev. A 47 (1993), p. 3554.

[41] J.C. Bergquist, W.M. Itano, and D.J. Wineland, *Recoilless optical absorption and Doppler sidebands of a single trapped ion*, Phys. Rev. A 36 (1987), p. 428.

[42] F. Schmidt-Kaler, S. Gulde, M. Riebe, T. Deuschle, A. Kreuter, G. Lancaster, C. Becher, J. Eschner, H. Häffner, and R. Blatt, *The coherence of qubits based on single Ca$^+$ ions*, J. Phys. B 36 (2003), p. 623.

[43] A.H. Myerson, D.J. Szwer, S.C. Webster, D.T.C. Allcock, M.J. Curtis, G. Imreh, J.A. Sherman, D.N. Stacey, A.M. Steane, and D.M. Lucas, *High-fidelity readout of trapped-ion qubit*, Phys. Rev. Lett. 100 (2008), 200502.

[44] M. Acton, K.-A. Brickman, P.C. Haljan, P.J. Lee, L. Deslauriers, and C. Monroe, *Near-perfect simultaneous measurement of a qubit register*, Quantum Inf. Comput. 6 (2006), p. 465.

[45] M.J. McDonnell, J.-P. Stacey, S.C. Webster, J.P. Home, A. Ramos, D.M. Lucas, D.N. Stacey, and A.M. Steane, *High-efficiency detection of a single quantum of angular momentum by suppression of optical pumping*, Phys. Rev. Lett. 93 (2004), 153601.

[46] C. Wunderlich, T. Hannemann, T. Körber, H. Häffner, C.F. Roos, W. Hänsel, R. Blatt, and F. Schmidt-Kaler, *Robust state preparation of a single trapped ion by adiabatic passage*, J. Mod. Opt. 54 (2007), p. 1541.

[47] A. Keselman, Y. Glickman, N. Akerman, S. Kotler, and R. Ozeri, *High-fidelity state detection and tomography of a single ion Zeeman qubit*, New J. Phys. 13, (2011), 073027.

[48] T. Schaetz, M.D. Barrett, D. Leibfried, J. Britton, J. Chiaverini, W.M. Itano, J.D. Jost, E. Knill, C. Langer, and D.J. Wineland, *Enhanced quantum state detection efficiency through quantum information processing*, Phys. Rev. Lett. 94 (2005), 010501.

[49] D.B. Hume, T. Rosenband, and D.J. Wineland, *High-fidelity adaptive qubit detection through repetitive quantum nondemolition measurements*, Phys. Rev. Lett. 99 (2007), 120502.

[50] D.J. Wineland, *Quantum entanglement and information processing*, in *Proceedings of the Summer School in Les Houches, Session LXXIX, 2003*, D. Estève, J.M. Raimond, and J. Dalibard, eds., Elsevier, Amsterdam, 2004, pp. 261–294.

[51] F. Mintert and C. Wunderlich, *Ion-trap quantum logic using long-wavelength radiation*, Phys. Rev. Lett. 87 (2001), 257904.

[52] J. Chiaverini and W.E. Lybarger, Jr., *Laserless trapped-ion quantum simulations without spontaneous scattering using microtrap arrays*, Phys. Rev. A 77 (2008), 022324.

[53] C. Ospelkaus, C.E. Langer, J.M. Amini, K.R. Brown, D. Leibfried, and D.J. Wineland, *Trapped-ion quantum logic gates based on oscillating magnetic fields*, Phys. Rev. Lett. 101 (2008), 090502.

[54] M. Johanning, A. Braun, N. Timoney, V. Elman, W. Neuhauser, and C. Wunderlich, *Individual addressing of trapped ions and coupling of motional and spin states using rf radiation*, Phys. Rev. Lett. 102 (2009), 073004.

[55] C. Ospelkaus, U. Warring, Y. Colombe, K.R. Brown, J.M. Amini, D. Leibfried, and D.J. Wineland, *Microwave quantum logic gates for trapped ions*, preprint (2011). Available at arXiv:1104.3573v2.

[56] R. Ozeri, W.M. Itano, R.B. Blakestad, J. Britton, J. Chiaverini, J.D. Jost, C. Langer, D. Leibfried, R. Reichle, S. Seidelin, J.H. Wesenberg, and D.J. Wineland, *Errors in trapped-ion quantum gates due to spontaneous photon scattering*, Phys. Rev. A 75 (2007), 042329.

[57] R. Ozeri, C. Langer, J.D. Jost, B. DeMarco, A. Ben-Kish, B.R. Blakestad, J. Britton, J. Chiaverini, W.M. Itano, D.B. Hume, T. Rosenband, P.O. Schmidt, and D.J. Wineland, *Hyperfine coherence in the presence of spontaneous photon scattering*, Phys. Rev. Lett. 95 (2005), 030403.

[58] H. Uys, M.J. Biercuk, A.P. VanDevender, C. Ospelkaus, D. Meiser, R. Ozeri, and J.J. Bollinger, *Decoherence due to elastic Rayleigh scattering*, Phys. Rev. Lett. 105 (2005), 200401.

[59] M.V. Berry, *Quantal phase factors accompanying adiabatic changes*, Proc. Roy. Soc. London 392 (1984), p. 45.

[60] Y. Aharonov and J. Anandan, *Phase change during a cyclic quantum evolution*, Phys. Rev. Lett. 58 (1987), p. 1593.

[61] J.I. Cirac and P. Zoller, *A scalable quantum computer with ions in an array of microtraps*, Nature 404 (2000), p. 579.

[62] S.-L. Zhu and Z.D. Wang, *Unconventional geometric quantum computation*, Phys. Rev. Lett. 91 (2003), 187902.

[63] P.J. Lee, K.-A. Brickman, L. Deslauriers, P.C. Haljan, L.-M. Duan, and C. Monroe, *Phase control of trapped ion quantum gates*, J. Opt. B 7 (2005), p. S371.

[64] D.F.V. James, *Quantum dynamics of cold trapped ions with application to quantum computation*, Appl. Phys. B 66 (1998), p. 181.

[65] M.J. McDonnell, J.P. Home, D.M. Lucas, G. Imreh, B.C. Keitch, D.J. Szwer, N.R. Thomas, S.C. Webster, D.N. Stacey, and A.M. Steane, *Long-lived mesoscopic entanglement outside the lamb-dicke regime*, Phys. Rev. Lett. 98 (2007), 063603.

[66] P.C. Haljan, P.J. Lee, K.-A. Brickman, M. Acton, L. Deslauriers, and C. Monroe, *Entanglement of trapped-ion clock states*, Phys. Rev. A 72 (2005), 062316.

[67] A. VanDevender, Y. Colombe, J. Amini, D. Leibfried, and D.J. Wineland, *Efficient fiber optic detection of trapped ion fluorescence*, Phys. Rev. Lett. 105 (2010), 023001.

[68] D. Aharonov and M. Ben-Or, *Fault tolerant quantum computation with constant error*, preprint (1996). Available at arXiv:quant-ph/9611025v2.

[69] J. Preskill, *Reliable quantum computers*, Proc. R. Soc. Lond. A 454 (1998), p. 385.

[70] E. Knill, *Quantum computing with realistically noisy devices*, Nature 434 (2005), p. 39.

[71] E. Knill, D. Leibfried, R. Reichle, J. Britton, R.B. Blakestad, J.D. Jost, C. Langer, R. Ozeri, S. Seidelin, and D.J. Wineland, *Randomized benchmarking of quantum gates*, Phys. Rev. A 77 (2008), 012307.

[72] K.R. Brown, A.C. Wilson, Y. Colombe, C. Ospelkaus, A.M. Meier, E. Knill, D. Leibfried, and D.J. Wineland, *Single-qubit gate error below 10^{-4} in a trapped ion*, preprint (2011). Available at arXiv: 1104.2552v1.